Plant Cell Reports (2025) 44:156
https://doi.org/10.1007/s00299-025-03546-2

ORIGINAL ARTICLE

Female gametophyte development, pollen−pistil interactions and embryogenic patterns in chicory (*Cichorium intybus*): a self-incompatibility perspective

Samela Draga[1] · Fabio Palumbo[1] · Damiano Riommi[1] · Marta Adelina Mendes[2] · Alex Cavalleri[2] · Giovanni Gabelli[1] · Silvia Farinati[1] · Alessandro Vannozzi[1] · Gianni Barcaccia[1]

Received: 24 April 2025 / Accepted: 5 June 2025 / Published online: 25 June 2025
© The Author(s) 2025

Abstract

Key message **Cytological and molecular investigations in chicory revealed crucial aspects related to female gametophyte development, pollen−stigma interactions, and self-incompatibility responses.**

Abstract The Asteraceae family, one of the largest of angiosperms, comprises approximately 24,000 species and exhibits considerable variation in reproductive biology. *Cichorium intybus* (commonly known as chicory) is among the most well-known and widespread species of the family. In addition to its economic and commercial value, chicory is considered one of the most interesting species in its family for the study of sporophytic self-incompatibility (SSI). Information regarding megasporogenesis, megagametogenesis, pollen tube development, and embryogenesis in this species is almost entirely absent in the scientific literature. Using confocal laser scanning microscopy (CLSM), we conducted a detailed investigation of female gametophyte development, providing a comprehensive characterization of the cytological stages involved in megasporogenesis and megagametogenesis. To investigate the dynamics and timing of pollen tube development and pollen rejection, we microscopically examined the interactions between pollen and stigmas in both cross- and self-pollinated plants. The response was similar to those documented in other Asteraceae species with a 'semidry' type of stigma. Integrated RNA-seq analyses further highlighted transcriptional changes during self- and non-self-pollen recognition and led to the identification of potential candidate genes involved in pollen tube development and callose deposition (in the case of self-incompatibility reactions). In parallel, for the first time, we characterized both the embryogenesis process and embryo sac degeneration in a compatible and incompatible crosses, respectively.

Keywords Chicory · Female gametophyte · Pollen germination · Self-incompatibility · RNA-seq

Introduction

The Asteraceae family is one of the largest and most diverse plant families, encompassing approximately 24,000 species (Funk et al. 2005; Darqui et al. 2021). This taxon, alternatively known as the daisy family or Compositae, displays significant variation in its reproductive biology. As flowering plants, members of this family are heterosporous, producing two distinct types of spores that give rise to unisexual gametophytes: microspores and megaspores (Baterman and Di Michele 1994; Drews and Yadegari 2002; Drews and Koltunow 2011; Petersen and Burd 2017). To date, several cytological studies focused on the reproductive structure development in the Asteraceae family have been conducted on *Taraxacum*, *Senecio, Helianthus*, *Hieracium*, *Achillea*, *Ambrosia*, *Chrysanthemum*, *Ageratum*, *Pilosella*,

Communicated by Kinya Toriyama.

Samela Draga and Fabio Palumbo have contributed equally to this work.

✉ Gianni Barcaccia
gianni.barcaccia@unipd.it

[1] Department of Agronomy, Food, Natural Resources, Animals and Environment, University of Padova, 35020 Legnaro, PD, Italy

[2] Department of Biosciences, Università Degli Studi Di Milano, Via Celoria 26, 20133 Milan, Italy

Trichocline, *Erigeron*, *Lessingianthus* and *Cichorium* (Martinoli and Di Moisè 1963; Noyes and Allison 2005; Yurukova-Grancharova et al. 2006; Gotelli et al. 2008; Deng et al. 2010; Chehregani et al. 2011; Musiał and Kościńska-Pająk 2013; Franca et al. 2015; Chehregani and Salehi 2016; Janas et al. 2016, 2021; Elias et al. 2019; De Jesús Pérez et al. 2021). In *Cichorium intybus* L., the majority of studies have focused on male reproductive structures. The most comprehensive investigation was carried out by Habarugira et al. (2015), who examined the histomorphological changes occurring from flower initiation to anthesis. Male gametophyte development in chicory continues to attract research interest, primarily for the study of both nuclear and cytoplasmic male sterility mechanisms, which are widely used in breeding programs and F1 hybrid production (Pacini and Keijzer 1989; Varotto et al. 1996; Habarugira et al. 2015; Waegneer et al. 2023).

In contrast, female sporogenesis and gametogenesis, along with embryo development in chicory, have not yet been reported. Insights into these processes can help elucidate the molecular and cellular mechanisms governing ovule development, embryo sac viability, and fertilization success. Furthermore, research on female gametophyte development is particularly relevant for understanding reproductive barriers and seed production.

Similarly, the mechanisms governing the interaction between male and female gametophytes are still far from being fully understood. Under normal circumstances, the recognition between pollen grains and stigmatic papillae ensures the germination of the former and the delivery of germ cells to the female gametophyte through the rapid growth of the pollen tube (Zheng et al. 2018). However, in chicory and, more generally, in the Asteraceae family, self-incompatibility (SI) phenomena have been frequently observed, garnering significant research attention as crucial mechanisms for preventing self-fertilization and promoting genetic diversity by outcrossing (Kaothien-Nakayama et al. 2010; Barrett 2013; Pang and Saunders 2014; Ferrer and Good-Avila 2007; Faehnrich et al. 2015; Barcaccia et al. 2016; Bala et al. 2023). In *C. intybus*, SI is particularly pronounced and is characterized by the immediate rejection of self-pollen or pollen from incompatible crosses (Varotto et al. 1995; Castaño et al. 1997; Lucchin et al. 2008). In this SI mechanism, which is known to involve the sporophytic type (SSI), the ability of a pollen grain to germinate on the stigma surface is determined by the genotype of the parental sporophyte. Despite the importance of SI in chicory, few studies have thoroughly examined the dynamics of pollen germination and the associated SI response, and the transcriptional dynamics underlying the regulation of this mechanism remain completely unknown.

In this study, we aimed to bridge some of the abovementioned gaps. For the first time, we provide a comprehensive analysis of megasporogenesis, megagametogenesis, pollen–stigma interactions and embryogenesis in *C. intybus* var. *latifolium*. A timescale for pollen germination in compatible crosses was outlined, indicating that a range of 20 min to 4 h is required for a pollen tube to germinate and reach the ovary for fertilization. In parallel, RNA-seq analyses were integrated to investigate the transcriptional changes occurring in response to self- and non-self-pollen recognition. Furthermore, an in-depth investigation was conducted into embryogenic patterns following a timeframe ranging from 5 to 96 h, encompassing all the steps of regular embryogenesis (in the case of self-compatibility) and embryo sac degeneration (in the case of self-incompatibility). Our findings provide, for the first time, foundational insights into the reproductive biology of chicory, with a particular emphasis on the SSI from a cytological and molecular point of view. The results from these analyses are expected to provide new insights into the mechanisms underlying SI in chicory, opening avenues for future research and contributing to comparative studies within the Asteraceae family, in which significant variability in embryological patterns has been observed, without a consistent structural distinction from other angiosperms (Johri et al. 2013; Franca et al. 2015).

Materials and methods

Plants used and growing conditions

The plants were grown in the greenhouse of the "L. Toniolo" experimental farm of the University of Padova (Legnaro, Padova, Italy). Overall, 19 plants of *C. intybus* var. *latifolium* (commonly known as 'Radicchio') and two of *C. endivia* var. *crispum* were grown. For the var. *latifolium*, eight plants belonging to the 'Red of Verona' biotype, four 'Red of Chioggia', four 'Treviso Precoce', and three 'Treviso Tardivo' were used. Plant seeds were obtained from different breeding companies and sown in seed starting trays filled with common potting soil. Thirty-day-old seedlings were transferred into large plastic containers and grown until flowering. Figure 1 shows the characteristic inflorescence of chicories (Fig. 1a), the structure of individual florets (Fig. 1b), and the crosses performed, as well as the biotypes used for microscopy analysis, aniline blue staining, and RNA-seq molecular analysis (Fig. 1c).

CLSM analysis

To elucidate megasporogenesis and megagametogenesis, buds of *C. intybus* var. *latifolium*, the biotype 'Red of Verona' was sampled at nine different stages (S8–S16) on the basis of the classification of Habarugira et al. (2015), in which male gametophyte development was associated with

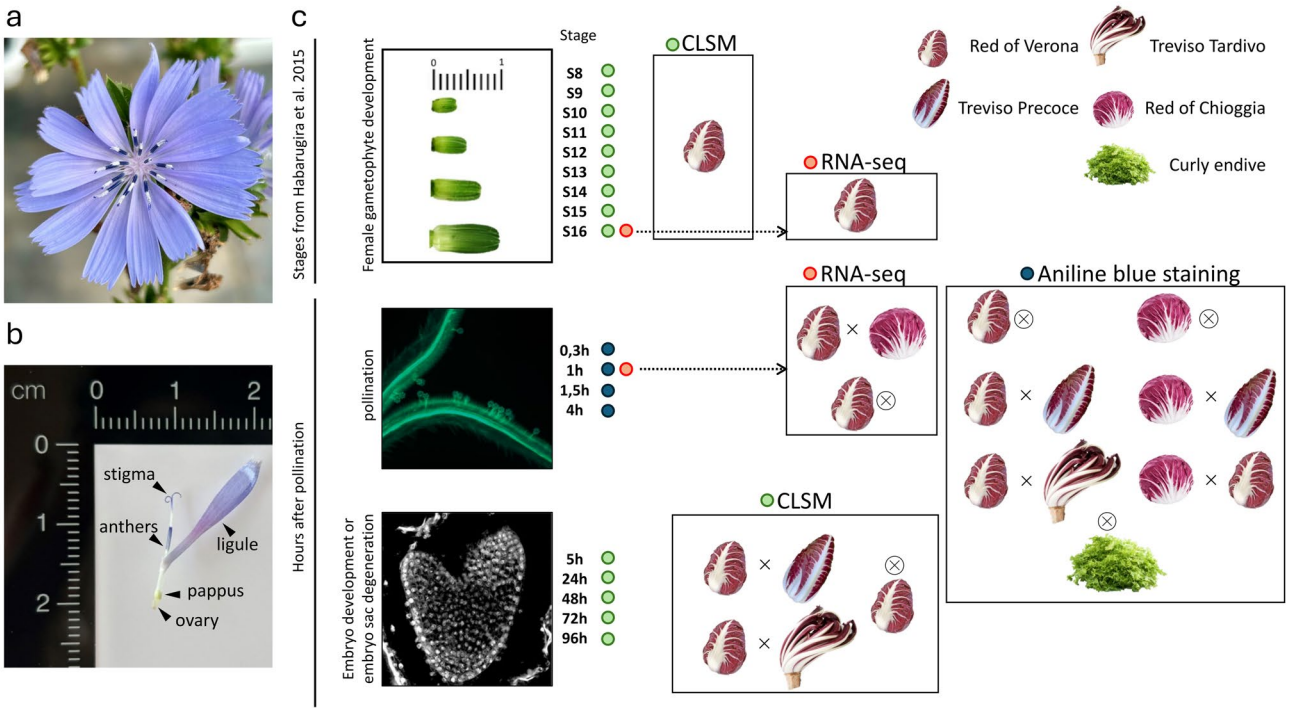

Fig. 1 Floral structure of chicory and experimental plan. **a** Chicory inflorescence. **b** Anatomy of a single floret. **c** Crosses performed and biotypes used in this study. For confocal laser scanning microscopy (CLSM) analysis, which was conducted to study megasporogenesis and megagametogenesis, *Cichorium intybus* var. *latifolium* 'Red of Verona' plants were used. The same methodology was applied to study both the early stages of embryogenesis (when 'Red of Verona' was crossed with 'Treviso Precoce' and 'Treviso Tardivo') and embryo sac degeneration following self-fertilization. To investigate pollen tube elongation/arrest through aniline blue staining, various combinations of crosses and self-fertilizations were performed. The transcriptional changes occurring after self- and cross-fertilization were evaluated in 'Red of Verona' stigmatic tissues via RNA-seq at three distinct stages: pre-pollination, 1 h after self-pollination, and 1 h after cross-pollination. In the latter case, pollen was taken from a 'Red of Chioggia' biotype. ⊗, self-pollination; ×, cross-pollination

specific stages of bud length. Self-pollination and cross-pollination were also conducted to investigate the first stages of embryogenesis (in the case of fertilization) or embryo sac degeneration (in the case of self-incompatibility or failed fertilization). At flowering, plants of the 'Red of Verona' biotype were always used as seed parents and pollinated by manually brushing self or nonself pollen onto their stigma. In addition to self-pollination, cross-pollination was carried out for the 'Red of Verona' × 'Treviso Precoce' and 'Red of Verona' × 'Treviso Tardivo' combinations. Each plant used for cross-pollination or self-pollination was kept in isolation cages before and after manual pollination, to avoid pollen contamination. Flowers were collected at 5 h, 24 h, 48 h, 72 h and 96 h postpollination (pp).

All samples were fixed overnight at 4 °C in FAA solution (3.7% formaldehyde, 5% acetic acid and 50% ethanol) and then prepared for Schiff's reagent staining overnight. The ovules were dissected under a drop of immersion oil (Sigma−Aldrich, Munich, Germany), and mounted on glass slides. For detection, the samples were excited using a laser (532 nm) with an emission between 570 and 740 nm via a Nikon A1 laser scanning confocal microscope (Nikon, Tokyo, Japan). The images were then processed using ImageJ software (Schneider et al. 2012).

Aniline blue staining

For in vivo pollen tube guidance experiments, once flowering was initiated and the stigma became receptive (in the early morning), manual cross-pollinations of *C. intybus* var. *latifolium* biotypes 'Red of Verona' × 'Treviso Precoce', 'Red of Verona' × 'Treviso Tardivo', 'Red of Chioggia' × 'Treviso Precoce', 'Red of Chioggia' × 'Red of Verona' and self-pollinations of 'Red of Verona', and 'Red of Chioggia' were conducted. Samples were collected after 20 min, 1 h, 1 h 30 min and 4 h after pollination to monitor the germination of the pollen tubes until they reached the ovary. As a reference, florets of *C. endivia* var. *crispum* (curly endive), a self-compatible species of *Cichorium*, were self-pollinated and sampled after 4 h. Pollination and plant isolation were performed as described in the previous section. The florets were then dissected from the capitula, and for each floret, the ligule was removed. They were then fixed in a mixture of acetic acid and absolute ethanol (1:3), washed three times with

water, cleared with 8 N sodium hydroxide and labeled with aniline blue after all the sodium hydroxide was removed via several washes with water. Microscopic observations were performed under a Nikon eclipse Ts2R microscope (Nikon, Tokyo, Japan), with inverted fluorescence. Whole pictures of the florets were acquired via the manual large capturing method.

RNA-seq analysis

Young leaves, anthers, and pollen were collected from four different plants (hereafter considered biological replicates) belonging to the *C. intybus* var. *latifolium* 'Red of Verona' biotype. Stigma tissues from the same four plants were also sampled at three distinct stages: pre-pollination, 1 h after self-pollination, and 1 h after cross-pollination. In the latter case, pollen was taken from a 'Red of Chioggia' biotype. Self- and cross-pollinations were conducted as previously described. All the tissues ($n = 24$) were snap-frozen in liquid nitrogen and stored at − 80 °C. Approximately 50 mg of each frozen tissue sample was ground in liquid nitrogen using a mortar and pestle, and total RNA was extracted using the RNeasy Plant Mini Kit (Qiagen, Hilden, Germany) according to the manufacturer's instructions. The RNA concentration was measured with both a Qubit 4 fluorometer (Qubit RNA BR Assay Kit, Thermo Fisher Scientific) and a NanoDrop-1000 spectrophotometer (Thermo Fisher Scientific), ensuring quality through 260/280 and 260/230 ratios. The integrity of the extracted total RNA was then confirmed via high-sensitivity RNA ScreenTape reagents on the 4150 TapeStation system (Agilent Technologies, MA, USA). Library preparation and sequencing (2 × 150 bp) were performed by Biomarker Technologies GmbH (BMKGene, Münster, Germany) using the NovaSeq 6000 platform (Illumina Inc. San Diego, CA, USA).

After demultiplexing, the quality of the raw reads was checked through MultiQC v1.13 (Ewels et al. 2016). Cutadapt v1.9 (Martin 2011) was used to trim low-quality reads with a Phred score below 30. The alignments were performed against the reference chromosome-scale assembly of *C. intybus* available from NCBI (GCA_023525715.1) (Fan et al. 2022). Bowtie2 v2.4.4 (Langmead and Salzberg 2012) was used at default parameters for read alignment, SAMtools v1.2 (Danecek et al. 2021) was used for sorting and indexing the alignment files, and bedtools multiCov v2.30.0 (Quinlan and Hall 2010) was used to generate the count matrix. An additional matrix was generated using TPM (Transcripts Per Million) normalization, to enable a comparison of expression levels between genes of the same sample. The R package *GenomicFeatures* (Lawrence et al. 2013) was employed to retrieve gene lengths from the genome annotation (GCA_023525715.1) (Fan et al. 2022). A custom R script was used to normalize the raw counts first based on gene length and then relatively to the total number of reads generated for sample, expressed in millions of reads.

Notably, the chicory reference genome lacked functional annotation (Fan et al. 2022). Therefore, for the genes and gene lists discussed in this study, an annotation was performed by searching for orthologous proteins in the reference genome of *A. thaliana* (Cheng et al. 2017). The protein sequences of chicory were used as queries and aligned (BLASTp) against the *Arabidopsis* proteome-based database (Mergner et al. 2020).

Coexpression network analyses were subsequently performed to identify clusters (modules) of highly correlated genes associated with specific tissues or developmental stages. The count matrix generated previously was initially filtered, retaining only those genes with more than 5 aligning reads in at least three samples. Data were normalized using the median of ratios method with the R package DESeq2 (Love et al. 2014), considering tissues as variables in the linear model. The same R package was also used to perform principal component analysis (PCA) and hierarchical clustering of the samples for an initial quality assessment. Weighted gene coexpression network analysis (WGCNA) was conducted on the normalized data, starting with hierarchical clustering using the blockwiseModules function from the R package WGCNA v1.70–3 (Langfelder and Horvath 2008). The following parameters were applied: net_type = signed, minModuleSize = 30, mergeCutHeight = 0.25, corType = Pearson, power = 8. The "power" threshold was determined using the pickSoftThreshold function, selecting the value that yields an R^2 value closest to 0.9. The resulting gene modules were further refined using k-means clustering with the applyKMeans function from the R package CoExpNets (Botía et al. 2017), with the following parameters: n.iterations = 50, net.type = signed, min.exchanged.genes = 20, excludeGrey = T. The modules showing the best correlation with the tissues under study, were further analyzed for module membership (MM) and gene significance (GS). Gene Ontology (GO) enrichment analysis was conducted for each identified module using the ShinyGO v0.80 tool (Ge et al. 2020).

The DESeq2-based normalized data were also used to identify DEGs with the R package DESeq2 (Love et al. 2014). Analyses were specifically performed to identify DEGs among pre-pollinated, self-pollinated and cross-pollinated stigma tissues. After the Benjamini−Hochberg method was applied (Benjamini and Hochberg 1995), genes with an adjusted p value (padj) lower than 0.05, were considered DEGs.

Results and discussion

Female gametophyte development

Most studies on the sporogenesis and gametogenesis are typically conducted in the more accessible male reproductive

structures. In contrast, analysis of female embryo sac development is particularly challenging because of the location of the cells within the nucellus and ovule tissues of the female flower (Barrell and Grossniklaus 2005). In chicory, building on the work of Habarugira et al. (2015), we analyzed nine developmental stages of buds, each corresponding to a specific event in a developmental male gametophyte. Our objective was to provide a comprehensive account of the events occurring during female gametophyte development, in accordance with the observations made for the male counterpart. To this end, we compiled Table 1, which aligns specific events occurring during sporogenesis and gametogenesis in chicory. Our data revealed that the beginning of the female gametophyte development occurs slightly later than that of the male gametophyte development: while the early pollen mother cell (PMC) is already visible at stage 7, the megaspore mother cell (MMC) appears only at stage 9. However, in the final stage of anthesis (stage 16), the two gametophytes align in synchrony, as they reach maturity.

Female gametophyte development is conventionally divided into two principal processes: megasporogenesis, which encompasses meiotic divisions of the megaspore mother cell (MMC), and megagametogenesis, which refers to the three mitotic divisions of the functional megaspore (FM) that give rise to the mature embryo sac (Yadegari and Drews 2004). These two processes occur in the developing ovule (Grossniklaus and Schneitz 1998; Yang and Sundaresan 2000; Barrell and Grossniklaus 2005).

In chicory, the ovule is of the anatropous type. Microscopic investigations by confocal imaging were performed from the initial stage of a young ovule with an archesporial cell, where the overall estimated perimeter of the ovule was 455 µm, and the funiculus length was 55 µm (Fig. 2a).

Compared with nearby cells, the emergence of the MMC near the micropylar end of the ovule was characterized by a large rectangular shape, and notably larger dimensions, with an estimated cell perimeter measuring 77.8 µm and a 30 µm nucleus perimeter (Fig. 2b). Interestingly, in this stage, a marked nucleolus located in the nucleus was easily detected, and an increase in the total perimeter of the ovule, reaching 554 µm, was observed. In Fig. 2c, an expanded MMC was observed (perimeter of 123 µm and a nucleus of 37 µm), with clearly visible chromosomes. The appearance of the diploid MMC marks the first stage of the megasporogenesis, which rapidly divides into completing the first meiosis, resulting in the formation of a dyad structure

Table 1 Histological events associated with a specific bud length and stage, from the study of Habarugira et al. (2015) with an association with the female counterpart, data produced from this study

Bud length (mm)	Stage	Events in male gametophyte (Habarugira et al. 2015)	Events in female gametophyte (this study)
1.2–1.4	7	Appearance of early pollen mother cells (PMC) and second parietal cell layer	*na*
1.5–2	8	Four distinguishable anther layers, approximately 50 pmc longitudinally aligned in each locule, enlargement and vacuolation of tapetum	Young ovule with archesporial cell
2–2.5	9	Callose deposition around PMC, meiosis	First appearance of megaspore mother cell (MMC)
2.5–3	10	Tetrads of microspores, crushing of middle layer by the enlarging tapetum, nuclear division in tapetum cells	First meiosis of the MMC and dyad visualization with the cell plate formation
3–4	11	Degradation of callose, release of microspores, disappearance of middle layer, tapetal cell intrusion in the locule	Second meiosis, giving rise to a linear tetrad of megaspores
4–5	12	Vacuolate microspore, expansion of endothecium cells, start of septum disintegration	Degenerating megaspores in the micropylar end, the chalazal megaspore remains the functional megaspore (FM), FG1 stage
6	13	First pollen mitosis, start of starch accumulation in the pollen grain, secondary thickenings of endothecium cell wall, anthocyanin biosynthesis in the anther	Two-nucleate female gametophyte (FG3) entering the second mitosis Four-nucleate female gametophyte (FG4). Cells well positioned in the polar ends
7	14	Two-celled pollen grain, complete degeneration of tapetum	Eight-nucleate embryo sac in FG5, polar nuclei migrating toward the center to form the central cell
8–9	15	Tricellular pollen grain, completion of septum disintegration, stomium opening, release of pollen grains in the locule	FG6, the polar nuclei fused to form the central cell, and 7 cells are visible in the mature embryo sac
10–12	16	Anthesis, rapid elongation of the floral tube, pollen collection by the style brushing hairs	Mature embryo sac, FG7 stage, 7-celled embryo Central cell and egg cell more defined than in stage 15, and ready for fertilization

Na Not analyzed, *FG* female gametophyte

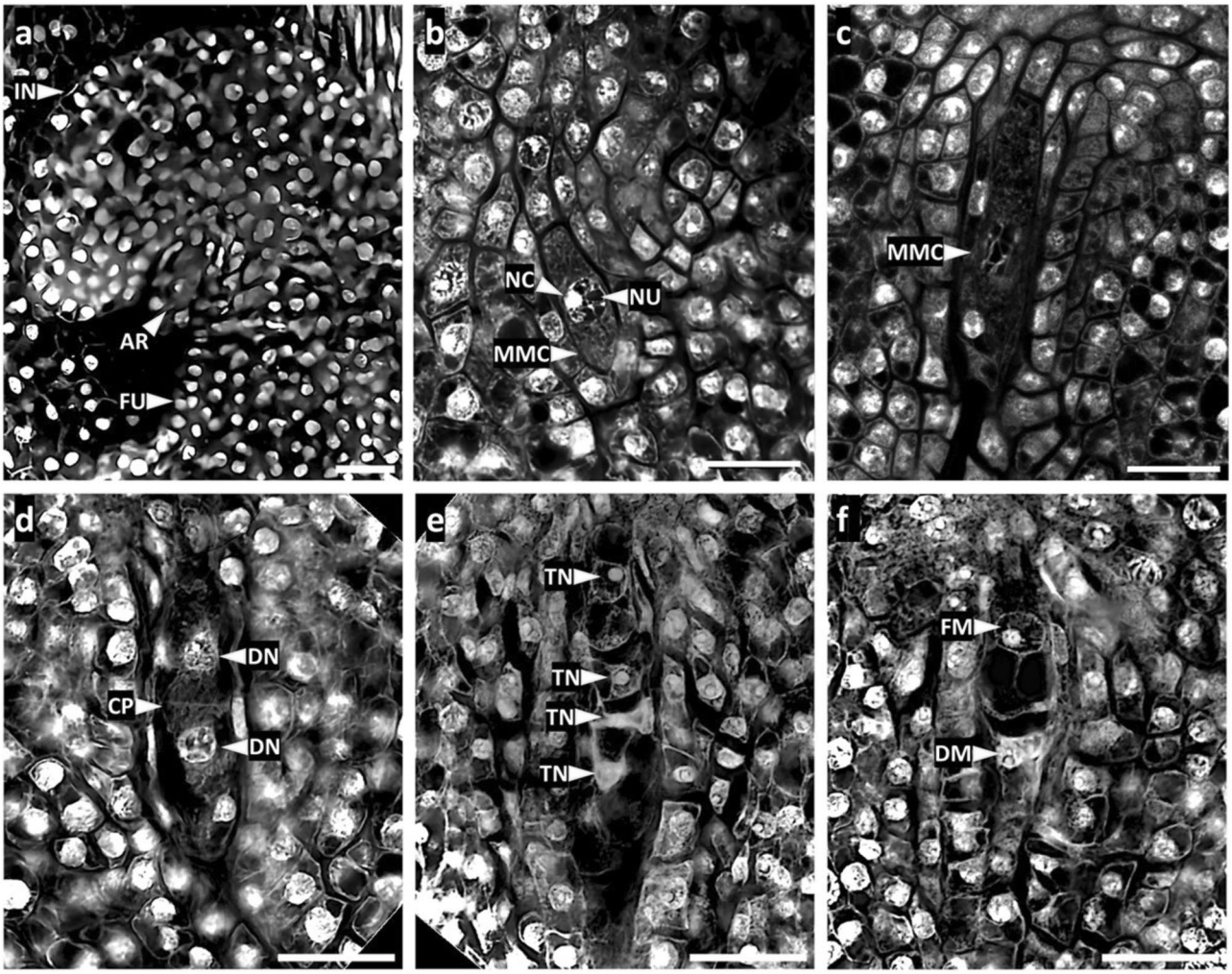

Fig. 2 Megasporogenesis in *C. intybus*. **a** Young ovule structure with an archesporial cell (*AR*). **b** Megaspore mother cell (*MMC*) with a large nucleus (*NU*) positioned toward the micropylar end. **c** The *MMC* with chromosomes clearly visible in the nucleus **d** Dyad stage. **e** Linear tetrad of megaspores. **f** Functional megaspore (*FM*) at the chalazal end and the degenerated nuclei in the micropylar end. *IN* Integument, *FU* Funiculus, *NC* Nucleolus, *DN* Dyad nuclei, *CP* Cell plate, *TN* Tetrad nuclei, *DM* Degenerated megaspores. Scale bars: 20 µm

(dyad perimeter: 135 µm, both nuclei: 20 µm), comprising two cells divided by the cell plate visible in Fig. 2d. From this point onwards, the dyad is oriented such that one cell is located toward the chalazal end, whereas the other is positioned toward the micropylar end. The dyad subsequently enters the second meiosis, developing a tetrad structure with a total perimeter of 156 µm (Fig. 2e). One of the megaspores of the tetrad (perimeter 132 µm), situated at the chalazal end, subsequently develops into the FM with a nucleus perimeter of 25 µm, whereas the other three megaspores degenerate at the micropylar end (Fig. 2f).

During megagametogenesis, the surviving megaspore undergoes three mitotic divisions to form the mature female gametophyte (FG), which is also known as the embryo sac or megagametophyte. The development process of FGs can be divided into seven distinct stages, designated as FG1 to FG7, on the basis of the model described in *Arabidopsis* by Christensen et al. (1997). In the present study, we report the corresponding stages, except for FG2. However, FG2 and FG3 represent both stages of a two-nucleate embryo sac that results from the first mitosis of the FM (Christensen et al. 1997). The distinction between these two stages is that in FG2, the two resulting nuclei from the first division of the FM are positioned in the center of the embryo sac, whereas in FG3, the two nuclei are positioned at the polar ends and separated by a vacuole, prepared to undergo a second mitosis (Fig. 3a).

The two subsequent mitotic divisions result in the formation of a four-nucleate embryo sac in FG4 (Fig. 3b) and in an eight-nucleate embryo sac in FG5 (Fig. 3c, d).

The mature embryo sac in chicory (FG6, FG7; Fig. 3e, f, respectively), as in the case of numerous species within the Asteraceae family, conforms to the typical Polygonum type. During cellularization, the eight nuclei give rise to seven cells: an egg cell, and two synergid cells at the micropylar end, a large diploid central cell in the central region, and three antipodal cells at the chalazal end. Despite considerable efforts to elucidate the precise mechanisms governing cell type differentiation within the female gametophyte and to distinguish the egg cell from the synergid cells, these issues remain largely unresolved. Research in *Arabidopsis* has shown that the spatial patterning of the embryo sac is influenced by asymmetric auxin distribution (Pagnussat et al. 2009). Additionally, nuclear positioning has been proposed as a key factor in the specification of the egg apparatus (Sun et al. 2021).

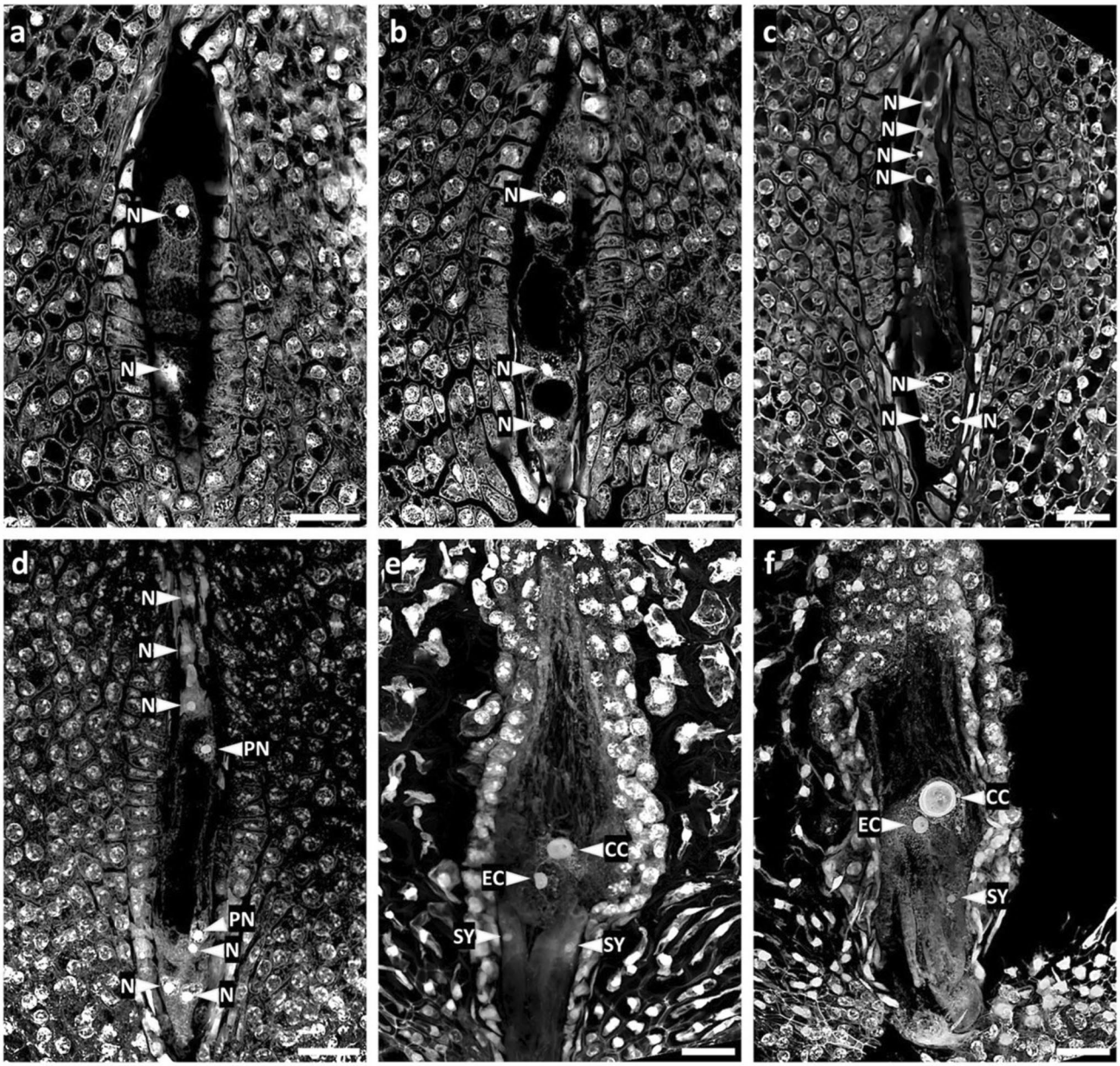

Fig. 3 Megagametogenesis in *C. intybus*. **a** Stage FG3, the binucleated embryo sac enters the second mitosis. **b** Stage FG4, tetra-nucleate embryo sac. **c** Early Stage FG5, vertical arrangement of the nuclei from the third mitosis (7 out of 8 cells are visible). **d** Late Stage FG5, the eight-nucleate embryo sac with the two polar nuclei migrating toward the center. **e** Stage FG6: Embryo sac during maturation with a small central cell, image obtained from the maximum intensity Z projection. **f** Stage FG7, mature embryo sac with an enlarged central cell, image obtained from the maximum intensity Z projection. *N* Nuclei, *PN* Polar nuclei, *AC* Antipodal cell, *EC* Egg cell, *SY* Synergid, *CC* Central cell. Scale bars: 20 µm

In the mature embryo sac, an increase in the size of the central cell was observed, whereas three antipodal cells were not observed (Fig. 3f). In some cases, two antipodal cells were detected, but since they were in a different plane, they could not be shown in the images. However, they can be observed in Supplementary Video 1, which shows a mature embryo sac, with two antipodal cells out of three. In many species, including *Arabidopsis*, antipodal cells are known to undergo programmed cell death (PCD) or reduce in size before fertilization (Kägi et al. 2010; Sprunck and Groß-Hardt 2011; Heydlauff and Groß-Hardt 2014; Van Hautegem et al. 2015). Among the Asteraceae family, studies in *Achillea* species revealed that most antipodal cells degenerate during the late stages of embryo sac development although complete degeneration is not consistently observed (Chehregani and Salehi 2016). In *Chrysanthemum* species, antipodal cells remain viable after egg apparatus formation, whereas in *Calendula officinalis*, degeneration begins prior to egg apparatus formation (Ao 2007; Deng et al. 2010). These findings suggest significant variability in antipodal cell fate with respect to size, number, and timing of degeneration within Asteraceae species (Gotelli et al. 2008; Deng et al. 2010). However, the inferred degeneration of antipodal cells raises questions about whether cell disappearance represents true degeneration or a detection limitation (Song et al. 2014).

Although the function of antipodal cells remains poorly characterized, research efforts have focused on elucidating the function of synergids. Synergids are thought to be crucial in the fertilization process, attracting pollen tubes to egg cells. Among the two mature synergids, only one, termed the receptive synergid, receives the pollen tube, whereas the other is referred to as the persistent synergid (Mogensen 1984; Higashiyama 2002; Higashiyama and Takeuchi 2015; Maruyama and Higashiyama 2016).

Overall, many molecular mechanisms remain to be clarified, particularly with respect to cell differentiation, central cell formation, synergid-mediated pollen tube guidance, and the function of antipodal cells. Understanding these processes will provide insights into plant reproductive development.

To evaluate and measure the difference between the nuclei of the cell of an embryo sac, estimation of their perimeter and area was conducted (Fig. 4).

The observable nuclei in five mature embryo sacs (in FG6 and FG7), were illustrated in a graphical representation by analyzing the perimeter and area correlation in Fig. 4a and, singularly, in box plots of the nuclear area (Fig. 4b) and perimeter (Fig. 4c)**.** A significant disparity in the nuclear area and perimeter was observed among the embryo sac cell types. The central cell nuclei exhibited the largest dimensions, followed by those of the egg cells. For both the nuclear area (Fig. 4b) and perimeter (Fig. 4c), the most prominent differences were found between the central cell and both synergid and antipodal cells, with the egg cells also differing significantly from the antipodal cells. Though differences were observed among the nuclei of embryo sac cells, their biological significance remains unknown due to the absence of comparable measurements in the literature.

Pollen tube germination

Aniline blue staining has been used as a rapid and dependable technique for the identification of callose deposition, particularly in the context of pollen tube growth (Eschrich and Currier 1964). This technique uses a fluorochrome that specifically binds to callose, allowing for its visualization via fluorescence microscopy using an ultraviolet (UV) filter (Mason et al. 2020). The molecular mechanisms underlying pollen tube growth are particularly puzzling as it is the only cell type in which plant cell growth is extremely rapid and confined to the tip of the cell (Chebli and Geitmann 2007; Bove et al. 2008; Hepler et al. 2013). The structure of a chicory floret, as observed through fluorescence microscopy, is shown in Fig. 5a.

The florets of chicory are situated within the capitula, with a typical number of 15–25 per inflorescence, and are encircled by a series of bracts, forming an involucre (M Kiers 2000; Mathieu et al. 2020). As the pistil matures, the style and the stigma extend through the tube formed by five fused anthers. During the aniline blue staining protocol, bleaching with sodium hydroxide renders the anthers more fragile, causing them to separate and increasing their visibility, as shown in Fig. 5a. Chicory florets are protandrous, a phenomenon characterized by the earlier maturation of male reproductive organs relative to female reproductive organs, reducing in this means self-pollen (Lloyd and Webb 1977; Bawa and Beach 1981; Forrest 2014). Indeed, the stigma of chicory comprises a receptive part of the papillae cells, which remain closed and hidden as they elongate and emerge from the anther tube (where mature pollen is present), preventing the receptive surface of the stigma from receiving self-pollen, whereas the outer side is composed of fake papillae cells, incapable of perceiving pollen. Upon extrusion of the stigma from the anther tube, the receptive portion of the papillae cells becomes exposed (Fig. 5b), thereby enabling the reception of potentially compatible pollen.

The pappus structure, as a characteristic trait in Asteraceae (M Kiers 2000), was easily detected and composed of diminutive scales (Fig. 5a, c, d). Moreover, in the inferior part of the pappus, a unilocular ovary was observed. This study reports, for the first time in chicory, the presence of a nectar structure at the base of the corolla, surrounding the style base (5d, e). The nectary structure is characterized by a star shape of round angles/tips with the presence of stomata, which are known to mediate nectar release (Fig. 5e) (Pacini

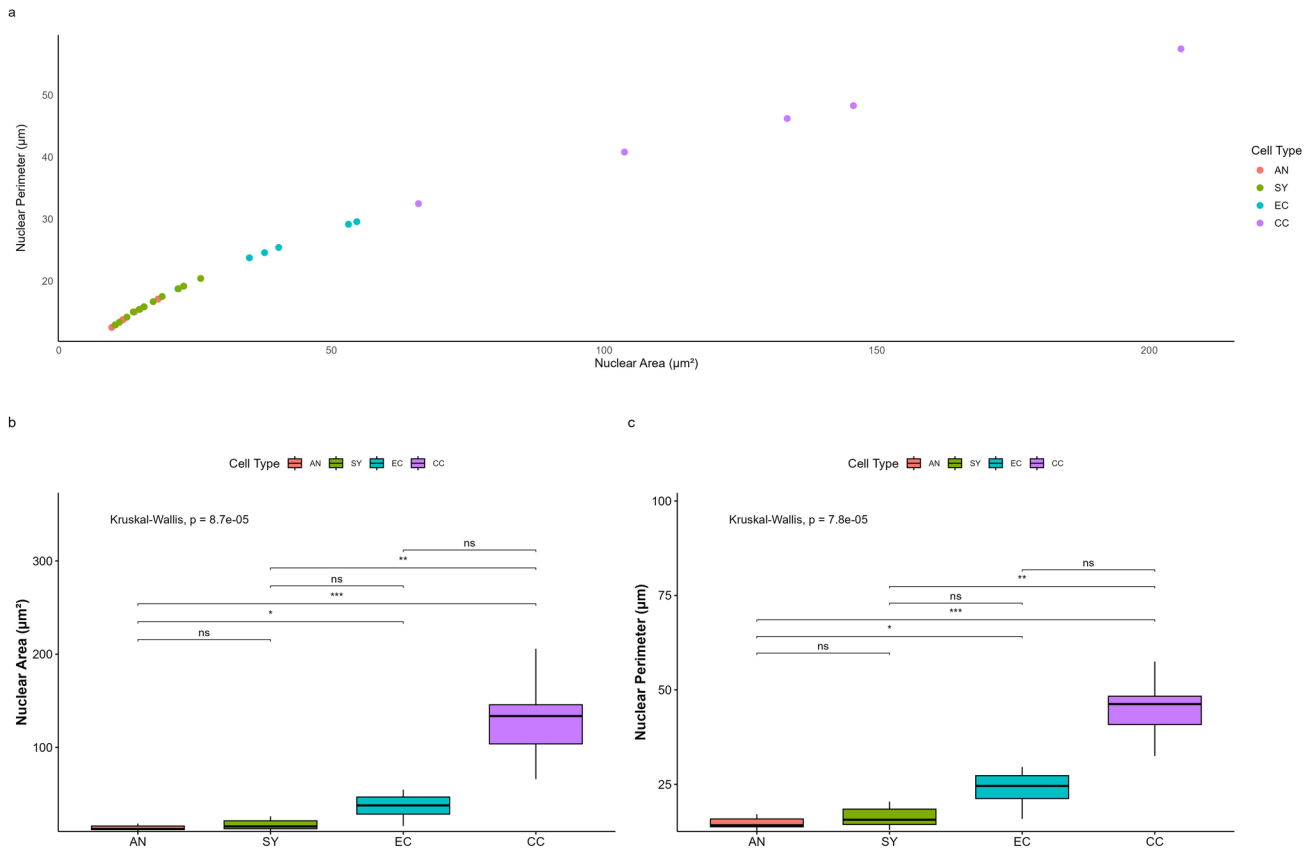

Fig. 4 Measurements of the nuclear area and perimeter of mature embryo sacs. **a** Scatter plot of the nuclear perimeter (µm) vs. nuclear area (µm^2) across different cell types **b** Boxplot of the nuclear area (in µm^2). **c** Nuclear perimeter (in µm). The global statistical significance was assessed using the Kruskal−Wallis test, whereas pairwise comparisons were conducted using the Dunn test with Bonferroni correction for multiple testing. P-values were adjusted using the Bonferroni correction for pairwise comparisons. Significance levels are indicated by asterisks as follows: $p \leq 0.05 = *$, $p \leq 0.01 = **$, $p \leq 0.001 = ***$. "ns" indicates no significant difference ($p > 0.05$). *AN* Antipodals, *SY* Synergids, *EC* Egg cell, *CC* Central cell

et al. 2003). However, few investigations of the nectary structure of Asteraceae have been conducted, which, interestingly, is known to play a large role in plant affinity and taxonomy, since the nectary structure may differ in terms of shape and amount of nectar secretion even within the same family (Sulborska and Weryszko-Chmielewska 2007; Wist and Davis 2008; Sulborska 2011; Wojtaszek and Maier 2014).

On the other hand, for the pollen tube germination analysis, we conducted a series of preliminary tests to optimize the protocol and gain insight into the microscopic fluorescence characteristics of the chicory florets, since no previous studies, to our knowledge, have provided images or detailed explanations. At the outset of our investigation, we discerned that the vascular bundle: xylem and phloem tissue, exhibited autofluorescence (Fig. 6a-f), which may initially prove confusing when attempting to identify the transmitting tract.

Once the parameters and general structure of the florets were defined, the next step was to determine which crosses were compatible among the chicory varieties investigated in this study. Given that chicory exhibits SSI and that incompatible pollen tubes are arrested on the stigma surface, the detection of the pollen tubes in the transmitting tract was considered as a compatible cross. The biotypes under consideration were 'Red of Verona', 'Red of Chioggia', 'Treviso precoce', and 'Treviso tardivo'. Our observations revealed that no incompatibility was observed among the biotypes used. Therefore, a series of independent samplings were conducted to establish a baseline for the germination and growth of pollen tubes in cross-pollinated florets at four time points. The timescales were as follows: 20 min, 1 h, 1 h 30 min, and 4 h. The results were then subjected to a detailed analysis, which yielded the conclusions represented in Fig. 6. In the left panels (Fig. 6a, c, e, g), female tissues (i.e., stigma, style and ovary) from a pre-pollinated floret were used as a negative control, whereas the same female tissues following a compatible cross-pollination event are reported in the right panels. In the latter case, the initial observation of pollen germination occurred at 20 min pp (Fig. 6b), with penetration of

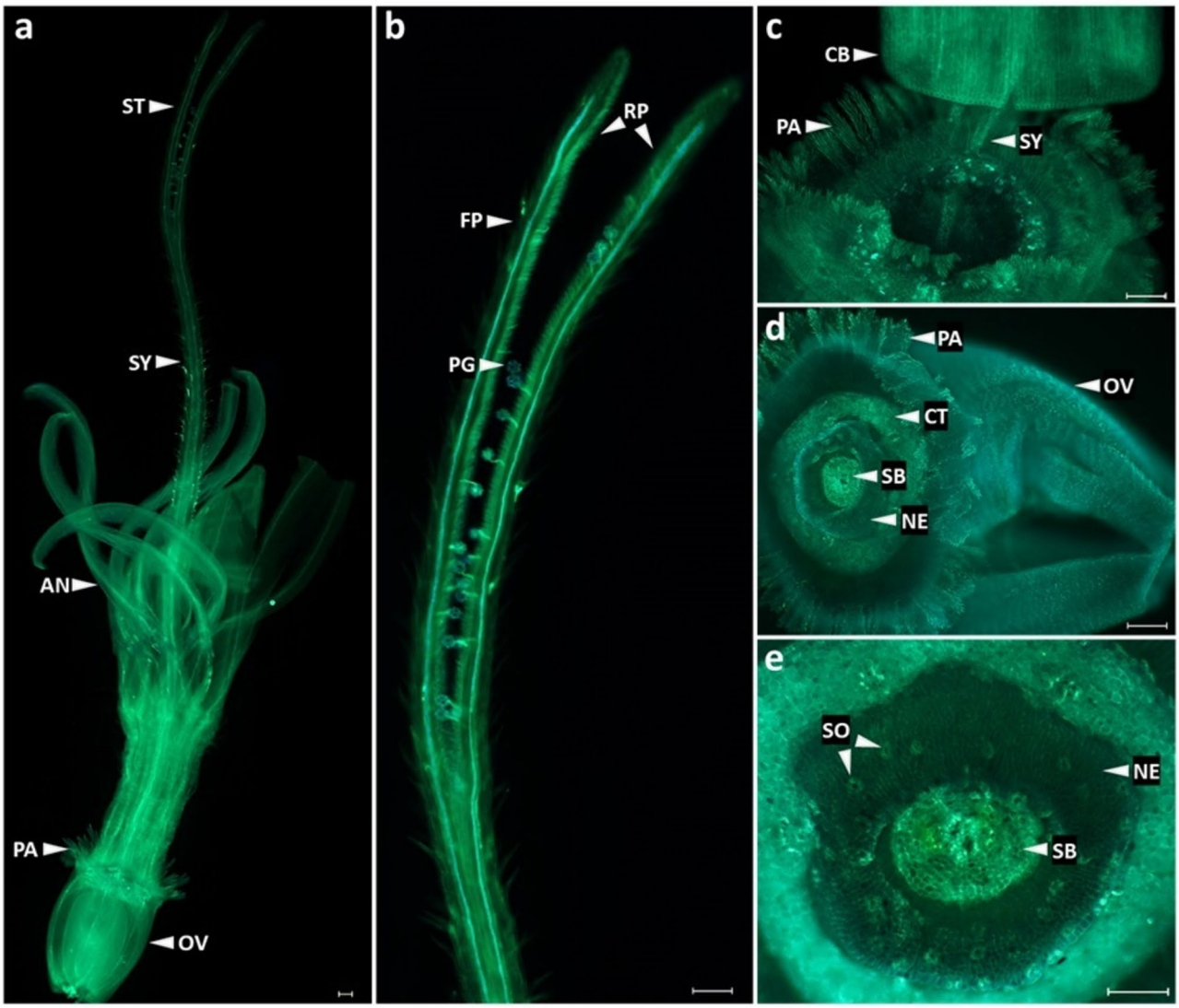

Fig. 5 Fluorescence microscopy of *C. intybus*. **a** Structure of a chicory floret with the ligule dissected prior to fixation. **b** Magnification of a pollinated stigma with grains (*PG*) adhering to receptive papillae (*RP*). Fake papillae (*FP*) and outer tissues of the stigma do not show any germinated pollen grains. **c** Corolla base (*CB*) detached from the lower part of the floret at the pappus structure level. **d** Closer look at the nectary (*NE*), surrounding the style base (*SB*). **e** Star-shaped nectary with the presence of stomata (*SO*). *ST* Stigma, *SY* Style, *AN* Anthers, *PA* Pappus, *OV* Ovary, *CT* Corolla tube. Scale bars: 100 µm

the stigma and growth of pollen tubes in the transmitting tract occurring at 1 h pp (Fig. 6d). The style and ovary were reached at 1 h and 30 min pp (Fig. 6f), and at 4 h pp, respectively (Fig. 6h). This finding suggests that within the 20 min to 1 h timeframe, pollen tubes in compatible crosses initially commence germination within the stigma papillae surface and subsequently undergo elongation but remain at the stigma level. Notably, in other Asteraceae species, such as *Senecio squalidus* and *Helianthus annuus*, pollen germination was observed to occur between 15 and 30 min in compatible crosses (Allen et al. 2011; Sharma and Bhatla 2013).

A comparative analysis of three different scenarios is presented in Fig. 7. Figure 7a and 7b and shows the stigma and the style of a floret subjected to self-pollination: pollen grains germinate but no pollen tubes penetrate the stigma or traverse the style. Callose deposits are distinctly visible on the receptive surface of the stigma. In contrast, Fig. 7c and 7d represent the stigma and style of a cross-pollinated floret: the pollen tube germinates and elongates in the transmitting tract. Finally, as shown in Fig. 7e and 7f, a floret from *C. endivia*, a self-compatible species, was used as a control, with pollen tubes exhibiting normal growth through the stigma and style tissues.

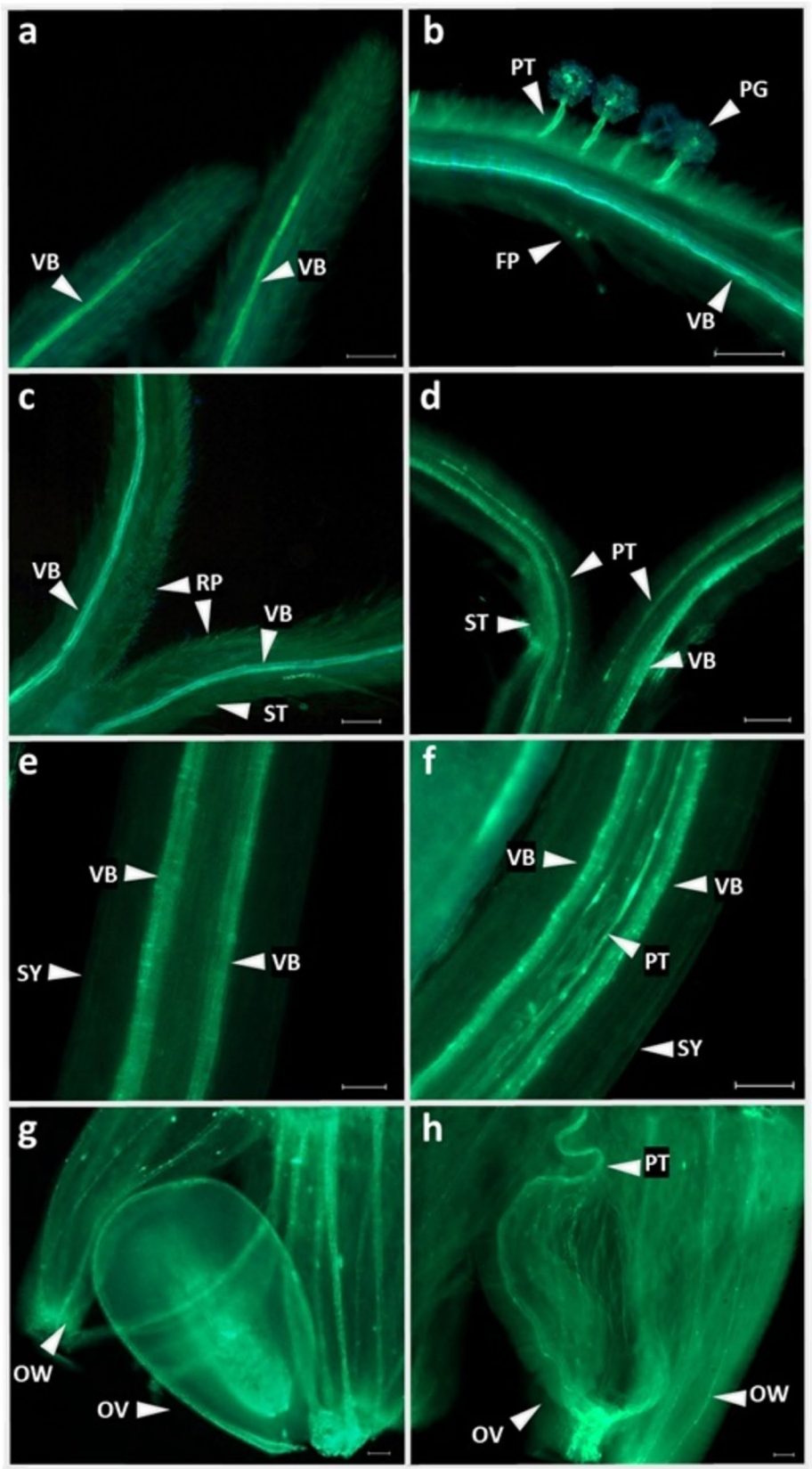

Fig. 6 Comparison of female tissues before pollination (negative control) and after compatible cross-pollination in chicory. In the left panels the pre-pollinated stage of: **a, c** stigma (*ST*), **e** style (*SY*), and **g** ovary (*OV*), were used as a negative control. Vascular bundles (*VB),* receptive papillae (*RP*), fake papillae (*FP*) and the ovary wall (*OW*) are indicated by arrows. The panels on the right show the pollen germination kinetics, following a compatible cross: **b** pollen grains (*PG*) either adhering to or germinating on the stigma surface 20 min post pollination (pp), **d** pollen tubes (*PT*) penetrating the stigma and elongating within the transmitting tract (*TT*) 1 h pp, **f** magnification of multiple pollen tubes advancing through the transmitting tract 1 h 30 min pp, and **h** pollen tubes reaching the ovary 4 h pp. Scale bars: 50 um

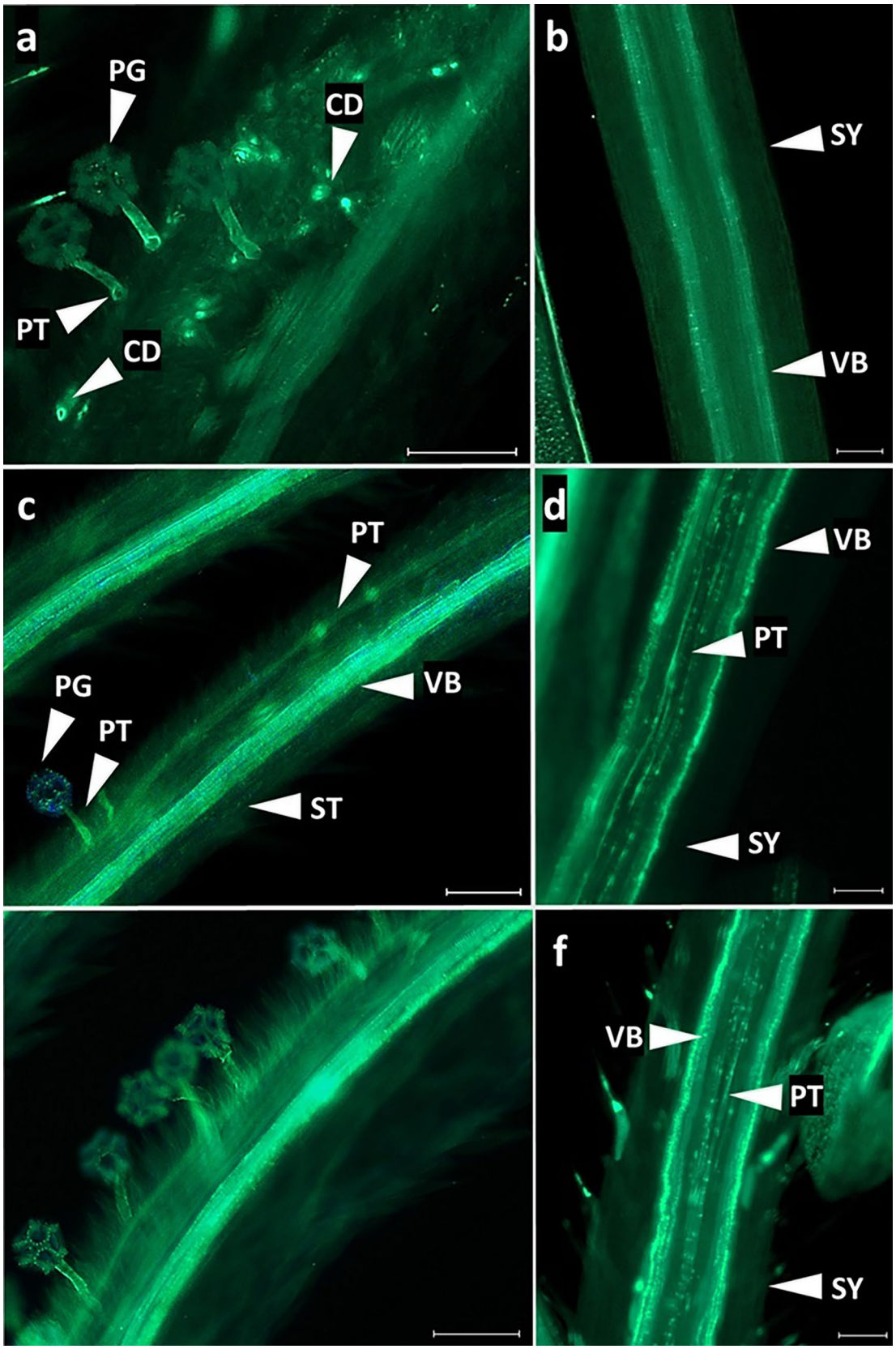
a
PG
CD
PT
CD
b
SY
VB
c
PT
PG
PT
VB
ST
d
VB
PT
SY
f
VB
PT
SY

◂**Fig. 7** **a, b** Self-pollination of chicory, **c, d** cross-pollination of chicory, and **e, f** self-pollination of endive**. a** Manually self-pollinated chicory, with arrested pollen tubes (*PT*), and callose deposits (*CD*) visible on the stigma (*ST*) surface. **b** Absence of pollen tubes in the chicory style (*SY*) following self-pollination; vascular bundles (*VB*), on the other hand, are clearly visible. **c** Pollen grain (*PG*) germination and pollen tube development through the stigma of (manually) cross-pollinated chicory. **d** Pollen tube growth within the chicory style following cross-pollination. The stigma (**e**) and style (**f**) of self-pollinated *C. endivia* (self-compatible), were used as positive controls. The pollen tube elongates in the transmitting tract, and callose deposits are not present. Scale bars: 50 µm

Pollen−stigma interactions are related mainly to the type of the stigma, as they were classified as either dry or wet on the basis of the presence or absence of secretions at the stigma surface (Heslop-Harrison and Shivanna 1977; Rejón et al. 2014; Bhatla and Lal 2023). According to earlier studies, SSI is associated with dry stigmas, whereas gametophytic SI is typically linked to wet stigmas, as initially described by Heslop-Harrison and Shivanna (1977). Wet stigmas typically secrete an exudate (extracellular secretion that covers the stigma outermost surface), which facilitates pollen germination. These stigmas generally lack a continuous cuticle, thereby enhancing the conditions for pollen germination (Dickinson 1995; Sang et al. 2012). Conversely, dry stigmas exhibit a greater degree of specificity, characterized by a continuous cuticle that significantly inhibits incompatible pollen tube germination, as in the case of SSI in *Brassica oleracea*, where self-pollen is immediately arrested, in most cases prior to germination (Dickinson 1995; Nasrallah 2023).

Elleman et al. (1992) conducted a comparative study of pollen−stigma interactions in five distinct species characterized by an SI response, including *Cosmos bipinnatus* and *Helianthus annuus* from the Asteraceae family. The authors reported that stigmas from these latter two SSI species do not appear to be completely dry, but rather seem to produce a small amount of surface secretion, allowing initial pollen tube growth even in the case of incompatible pollinations.

These observations were later substantiated by Hiscock et al. (2002), and Allen et al. (2010) in their detailed structural and cytological studies of the pollen−stigma interaction on *S. squalidus*, an Asteraceae member exhibiting SSI. From the germination trials of incompatible events in *S. squalidus*, three different scenarios were observed: i) pollen grains arrested prior to germination, or following the appearance of short pollen tube initials ii) pollen tubes arrested on the stigma surface, and iii) pollen tubes arrested after stigma penetration (on rare occasions). Callose deposition remains a common feature across all possible scenarios (Hiscock et al. 2002).

Further studies confirmed the nature of the semidry stigmas in other Asteraceae members, such as *Lessingianthus grandiflorus*, *Lucilia lycopodioides* (Teixeira et al. 2011), and *H. annuus* (Sharma and Bhatla 2013). For example, in this latter study, the pollen tube was also able to germinate in incompatible crosses, but failed to penetrate the papilla, instead continuing its growth parallel to it (Sharma and Bhatla 2013).

In many other Asteraceae species, such as *Ambrosia artemisiifolia* L. (Friedman and Barrett 2008), *Zinnia angustifolia* (Samaha et al. 1989), *Artemesia granatensis* (Peñas et al. 2011), and *Echinacea angustifolia* (Wist and Davis 2008), a comparable pattern was identified, with germinated pollen tubes (from self-pollination events or incompatible crosses) being arrested on the stigma surface.

Similarly, in chicory, pollen germination accompanied by callose deposition in self-pollinated stigmas was observed (Fig. 7a)**.** Since this event has rarely been observed in dry stigmas (Dickinson 1995; Hiscock et al. 2002), we hypothesize that chicory, like other Asteraceae species mentioned above, may exhibit a semidry stigma type. However, further cytochemical analysis is needed to determine whether chicory presents semidry stigmas, potentially indicating a shared trait within the Asteraceae family.

In many studies, pollen tube germination was monitored by observing the seed set, and/or, considering environmental conditions, the morphology of the flower (short/long style), pollen load, and pseudo self-incompatibility (Lloyd 1968; Eenink 1981; Burson 1987; Galen et al. 1989; Leduc et al. 1990; Varotto et al. 1995; Love et al. 2016). Several factors must be considered as errors may arise at various stages during these procedures. These potential sources of error include manual pollination techniques, seed counting accuracy, premature harvesting, misinterpretation of germinated pollen tubes on papillae cells as compatible pollinations, and challenges in detecting pollen tube elongation within the style (Eenink 1981; Faehnrich et al. 2015). From our perspective, the implementation of aniline blue methodology, comprising repeated analyses and the development of an optimized protocol, can ensure the production of reliable results. Following self-pollination and cross-pollination, we further explored both the transcriptomic changes occurring at the stigmatic level and the cytological changes occurring at the ovule level. The following sections will provide a detailed account of these observations.

Transcriptomic changes in stigma tissues pre-pollination, and following self- and cross-pollination

RNA-seq data were produced for young leaf (Leaf), anthers (Ant), pollen (Pol), pre (Pre-P), 1 h cross (Cross-P), and 1 h self (Self-P)-pollinated stigmas. The four biological replicates used for each tissue were derived from plants belonging to the 'Red of Verona' biotype, whereas the pollen used for cross-pollination was taken from 'Red of Chioggia'. Although the focus of our analyses was on stigmatic

tissues, we considered it useful to include anthers, leaves, and pollen to identify genes or gene clusters specific to stigmatic tissue and not expressed in the other tissues examined. Given the low number of reads, the fourth replicate of Pol tissue was excluded from further analyses. In total, approximately 972 M reads (on average 42 M reads per sample) were obtained, while, after the filtering steps, approximately 924 M reads were retained. After DESeq2 (Love et al. 2014) normalization, 40,884 genes were globally expressed in at least one tissue (Table S1). Pol presented the lowest number of expressed genes (24,792), whereas Cross-P presented the greatest number of expressed genes (34,702, Fig. 8A). For the evaluation of expression levels between genes within the same sample, we also provided an additional table with expression data normalized to TPM. (Table S2).

The PCA performed on DESeq2-normalized data (Fig. 8a) revealed a strong correlation among the replicates of each tissue, except for one of the three Pol biological replicates. Additionally, an overlap was observed between the biological replicates of Pre-P, Cross-P and Self-P. However, a certain degree of redundancy at the transcriptomic level was expected, considering that all samples were collected from the same tissue 1 h after self-pollination and cross-pollination events.

A WGCNA was then performed to identify clusters of genes (modules) sharing similar expression patterns. This method has become one of the most effective approaches for obtaining RNA-seq data from many plant species, but it has never been applied to chicory. The 44,884 expressed genes obtained after the DESeq2 normalization were initially used to construct a matrix with a soft-thresholding power of $\beta = 8$, ensuring a scale-free network. Setting the minimum module size to 30 (a module being a cluster of highly correlated genes), we identified 53 distinct modules. Modules with eigengenes (MEs, representing the expression profiles of all genes within a module) correlated above 0.25 were then merged, reducing the total number of modules to 31, each assigned a unique color. As suggested by Botía et al. (2017), we further applied a k-means step. This additional measure overcomes the limitations imposed by the exclusive use of a hierarchical clustering method (such as the WGCNA). A classical hierarchical method cannot reassign an expression vector already assigned to a specific cluster, even if its module centroid shifts significantly after the inclusion of additional vectors. The methodology proposed by Botía et al. (2017), hierarchically generates a draft of the modules, and then applies a k-means step starting from this draft, reassigning genes that were initially placed in the wrong module. Figure 8b shows the updated distribution of genes across the 31 modules after k-means clustering. Correlation analysis between the newly organized modules and the

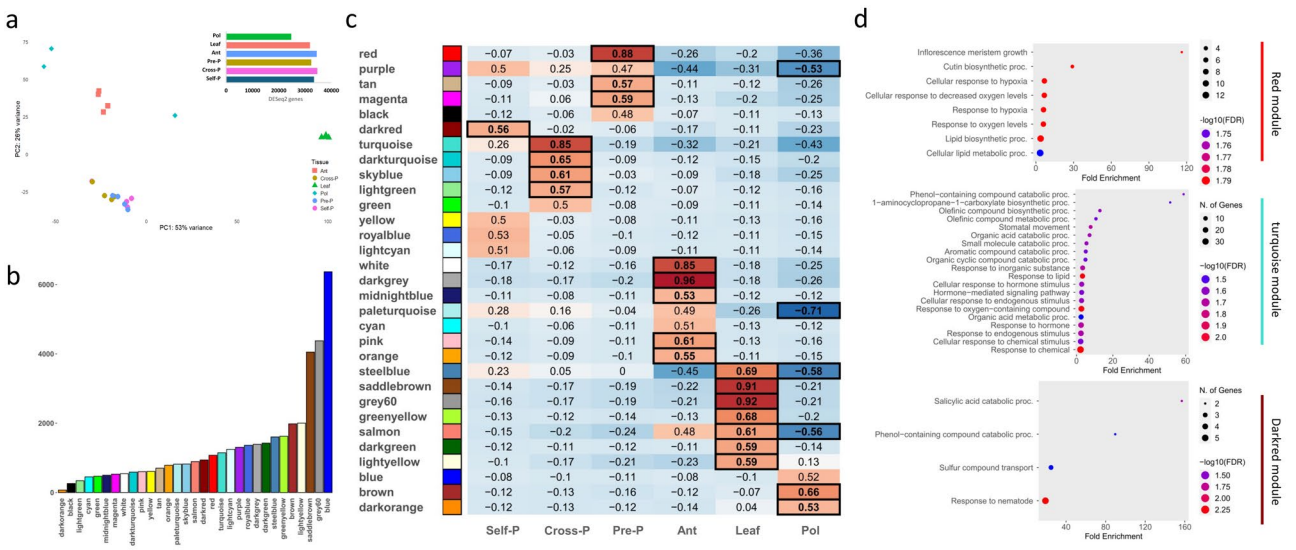

Fig. 8 WGCNA results. **a** PCA based on DESeq2-normalized data and, at the top right, the total number of DESeq2-based normalized genes for each of the six tissues under study (young leaf (Leaf), anther (Ant), pollen (Pol), pre (Pre-P), cross (Cross-P), and self (Self-P) -pollinated stigmas). For each of the six tissues, four biological replicates were used (with the exception of pollen, for which three replicates were used due to technical limitations). **b** WGCNA modules after the K-means clustering analysis. **c** Correlation analysis performed between the 31 WGCNA modules obtained after the K-means clustering analysis and the 6 tissues under study to identify highly tissue specific modules. The boxes with the thicker borders represent modules with a correlation p value < 0.01. **d** GO enrichment analysis (biological process category) of the genes contained in the three modules, namely, red, turquoise and dark red, which, according to Panel **c**, best correlated with Pre-P, Cross-P and Self-P tissues, respectively

six tissues under study revealed that one or more modules were highly correlated with each tissue (p value < 0.01). To investigate genes and molecular pathways involved in self-incompatibility and pollen tube growth, we focused mainly on stigma tissues (namely, Pre-P, Self-P and Cross-P), where the SSI components (male and female) are supposed to interact, determining whether pollen tube germination and development occur.

The red, the dark red, and the turquoise modules were specifically and significantly ($r = 0.88$, 0.56, and 0.85, respectively) correlated with Pre-P, Self-P and Cross-P stigma tissues, respectively (Fig. 8c). To explore whether the three abovementioned modules were enriched for genes falling within reproductive-related ontological categories, we conducted a gene set enrichment analysis (GSEA) on genes with a module membership (MM) and gene significance (GS) greater than 0.9 and 0.5, respectively. MM (between 0 and 1) reflects the association between a gene's expression profile and the module eigengene (ME), whereas GS (between -1 and 1) indicates the biological importance of a gene. In theory, genes with both high GS and MM values are likely to play key biological roles in the tissue correlated with their respective modules. Table S3 provides the MM and GS values for each gene assigned to the red, dark red, and turquoise modules in the WGCNA. The most enriched biological process (BP) categories included "inflorescence meristem growth" and "cutin biosynthetic process" for the red module, "phenol-containing compound catabolic process" and "1-aminocyclopropane-1-carboxylate biosynthetic process" for the turquoise module and "salicylic acid catabolic process" for dark red module (Fig. 8d). In the pre-pollinated stigma-associated red module, it was not surprising to find an enrichment of biosynthetic processes (BPs) linked to inflorescence meristem growth and to cutin and lipid biosynthetic processes. The outermost stigma layer is indeed a highly modified cuticle, which is mainly composed of cutin and lipids (Clifford and Owens 1990). In contrast, the enrichment of the BP category named "1-aminocyclopropane-1-carboxylate (ACC) biosynthetic process" in the Cross-P-correlating turquoise module was unique. Three genes belonging to this BP category were found to be members of the ACC-synthase (ACS) family, namely, *ACS1*, *ACS6* and *ACS8*. Weterings et al. demonstrated that pollination triggers a high and persistent accumulation of ACC oxidase (ACO) transcripts throughout all cells of the transmitting tract (Weterings et al. 2002). In contrast, ACC-synthase (ACS) mRNA accumulates only in a subset of transmitting tract cells, following a wave-like pattern, with the peak aligning with the advancing pollen tube tips. With respect to the enrichment of the salicylic acid (SA) catabolic process found in the dark red module, SA is known to be capable of regulating pollen tip growth (Rong et al. 2016) and callose synthesis/deposition, but studies elucidating the role of this phytohormone in the self-pollen recognition process are lacking (Wu et al. 2018).

Since none of the analyzed WGCNA modules were specifically enriched for BP categories related to pollen−pistil interaction or pollen tube development, we also analyzed the data from a different perspective. Through a classical DEG analysis, followed by enrichment analysis, we evaluated the changes that occurred at the transcriptomic level via pairwise comparisons of the three stigmatic tissues (Pre-P, Self-P and Cross-P stigmas; Table S4). Comparing pre-pollinated (Pre-P) to self- (Self-P) and cross-pollinated (Cross-P) stigmas, provides valuable insights into the molecular mechanisms governing pollen–pistil interactions, specifically callose production in the self-pollination events, or pollen tube initiation in case of cross-pollination. Moreover, the direct comparison between self- and cross-pollination (Self-P vs. Cross-P) offers a focused perspective on SSI, highlighting genes that are differentially expressed in stigmas at the same maturation stage and putatively involved in self-pollen rejection, pollen acceptance and pollen tube penetration.

In Fig. 9a and Fig. 9b**,** the genes significantly upregulated and downregulated (respectively) in each comparison are reported.

The number of exclusively upregulated and downregulated genes in the Self-P vs. Cross-P comparison was found to be 315 and 198, respectively (Fig. 9a and Fig. 9b). Notably, the most enriched categories among the downregulated genes were "response to stress" (GO: 0006950), "response to external stimulus" (GO:0009605), and "biological processes involved in interspecies interaction between organisms" (GO:0044419). This finding strengthens the hypothesis that the recognition of non-self-pollen and, more likely, the penetration of the stigma by the pollen tube seem to trigger the activation of elements involved in stress response pathways, as has been extensively demonstrated in other species (Hiscock and Allen 2008; Boavida et al. 2011; Mondragón-Palomino et al. 2017; Zhang et al. 2017). The number of downregulated genes in the Pre-P vs. Cross-P comparison (662, Fig. 9b) and in the Pre-P vs. Self-P comparison (1243, Fig. 9b) was clearly significantly greater than the number of upregulated genes in the same two pairwise comparisons (432 and 361, Fig. 9a). The analyses also revealed a substantial number of DEGs in both the Pre-P vs. Cross-P and Pre-P vs. Self-P comparisons. In particular, 1,344 genes (Fig. 9b) were downregulated in both comparisons. These data suggest that the interaction between pollen and the stigma leads to significant transcriptional changes as early as 1h after pollination, regardless of the type of pollen (self or nonself).

Focusing more closely on the process of pollen tube germination and growth, we identified 6 genes with *Arabidopsis* orthologues that fall into the "pollen tube guidance" BP category, namely, *MEE14*, *LIP*, and two copies of *NRX1*, *POP2* and *A36*. All of these genes were downregulated in at least

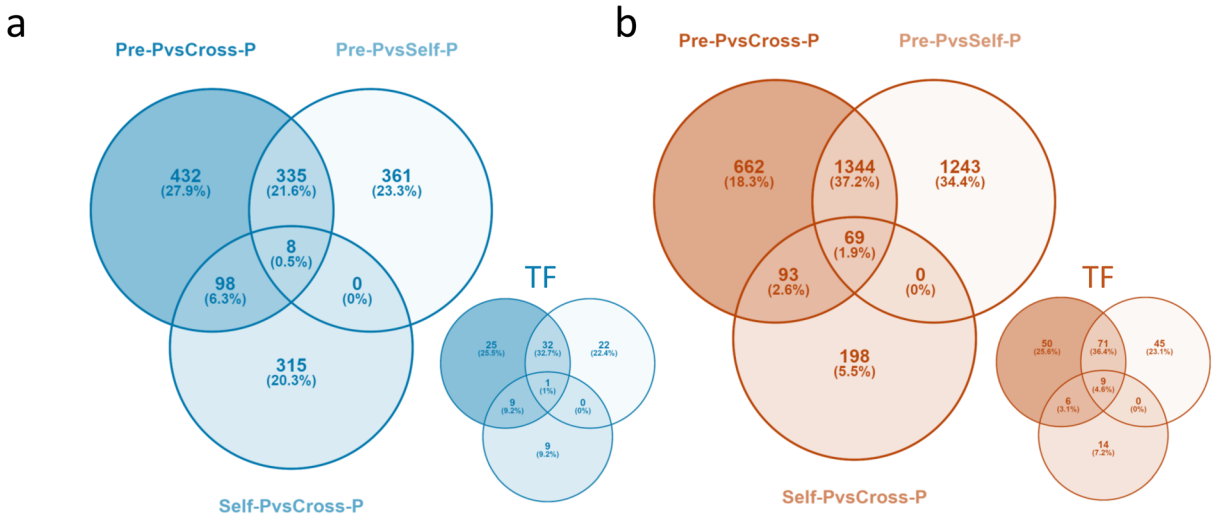

c

	Pre-P vs Cross-P		Pre-P vs Self-P		Self-P vs Cross-P		Arabidopsis	Function
Gene ID	Log2FC	adj-pval	Log2FC	adj-pval	Log2FC	adj-pval		
L2E82_25258	-5.25	3.48E-04	-6.25	1.56E-05			AT2G15890.1	*MATERNAL EFFECT EMBRYO ARREST 14 (MEE14)*
L2E82_22661	-4.96	3.60E-03					AT3G02810.1	*LIP (LOST IN POLLEN TUBE GUIDANCE 2)*
L2E82_42056	-3.35	1.49E-20	-2.12	5.23E-08	-1.22	1.79E-02	AT1G60420.1	*NRX1 (NUCLEOREDOXIN 1)*
L2E82_42057	-2.72	6.21E-17	-2.39	1.53E-12			AT1G60420.1	*NRX1 (NUCLEOREDOXIN 1)*
L2E82_08221	-3.60	1.31E-04	-4.62	4.74E-07			AT3G22200.1	*POLLEN-PISTIL INCOMPATIBILITY 2 (POP2)*
L2E82_21697	-1.88	1.43E-03					AT5G36260.1	*Aspartyl protease 36 (A36)*
L2E82_40935			-4.67	3.73E-03	4.41	2.41E-02	AT1G05570.2	*Callose synthase 1 (CALS1, GSL6)*
L2E82_42373			-5.05	1.10E-02			AT1G06490.2	*Callose synthase 7 (CALS7, GSL7)*
L2E82_29924			-2.34	2.78E-03			AT5G13000.1	*Callose synthase 3 (CALS3, GSL12)*
L2E82_17794					-4.68	7.13E-06	AT4G09960.2	*SEEDSTICK (STK)*

Fig. 9 DEG analysis. **a** Venn diagram showing specific and common upregulated genes in pairwise comparisons among the three stigmatic tissues (Pre-P, Self-P and Cross-P stigmas). In the bottom right, only the fraction of upregulated genes encoding transcription factors is shown. **b** Venn diagram showing specific and common downregulated genes in pairwise comparisons among the three stigmatic tissues (Pre-P, Self-P and Cross-P stigmas). On the bottom right, only the fraction of downregulated genes encoding transcription factors is shown. **c** Differentially expressed genes (in at least one of the three pairwise comparisons) that fell into the "pollen tube guidance" BP category or were associated with callose synthesis. For each gene, the log2FC values for the three pairwise comparisons (if adjusted *p* value < 0.05), the putative orthologues in *A. thaliana* and the putative functions are reported

one of the two comparisons, Pre-P vs. Cross-P or Pre-P vs. Self-P, whereas four were downregulated in both comparisons (Fig. 9c). Among the latter, we highlight L2E82_25258, the putative orthologous of *MATERNAL EFFECT EMBRYO ARREST 14* (*MEE14*, AT2G15890). The resulting protein, also known as CCG BINDING PROTEIN1 (CBP1), was found to interact with several other proteins, namely, CCG, NRPB1_CTD, MED7, MED9, several AGAMOUS-like (AGL) transcription factors, TBP1, and TFIIF, and to play a crucial role in pollen tube attraction (Li et al. 2015). L2E82_42056 and L2E82_42057 are two genes (putatively paralogues) that, on the basis of orthologous analysis with *A. thaliana*, could encode for *NUCLEOREDOXIN 1* (*NRX1,* AT1G60420). Mutations in *NRX1* cause defective pollen tube growth in the pistil (Qin et al. 2009). The role of this gene in pollen tube growth is further supported in chicory, where it was found to be overexpressed not only in the Cross-P vs. Pre-P and Self-P vs. Pre-P comparisons, but also in the Cross-P vs Self-P comparison. L2E82_08221 is the putative orthologous of *POLLEN-PISTIL INCOMPATIBILITY 2* (*POP2*, AT3G22200), which plays a role in mediating pollen tube guidance, as demonstrated by Palanivelu et al. (2003). *POP2* encodes a transaminase responsible for degrading γ-amino butyric acid (GABA), and in *pop2* flowers, GABA levels rise significantly, leading to a concentration-dependent disruption of pollen tube growth, guidance, and fertility. It was therefore hypothesized that GABA functions as an inhibitor of pollen tube elongation at high concentrations, and is a signal that guides pollen tube navigation. Finally, L2E82_22661 and L2E82_21697 were upregulated only in the Cross-P vs. Pre-P comparison. The first gene codes for *LOST IN POLLEN TUBE GUIDANCE 2*

(*LIP2*), a receptor-like kinase (RLK) that, along with LIP1, constitutes, a crucial component of the pollen tube receptor complex. Both the LIP1 and LIP2 proteins are localized at the tip of the pollen tube through palmitoylation, a process crucial for their role in guidance regulation. The simultaneous inactivation of these genes results in defective pollen tube guidance (Liu et al. 2013). The L2E82_21697 protein product is the putative orthologous of A36, an aspartyl protease, the knockout of which is responsible for a significant seed abortion and an apoptosis-like programmed cell death of pollen grains. In addition to A39, A36 is also involved in pollen tube guidance (Gao et al. 2017).

In addition to being a primary component of the cell wall surrounding developing microspores, callose also plays a key role in pollen tube growth (Kapoor and Geitmann 2023). Callose deposition in response to self or incompatible pollen grains acts as an impermeable barrier to pollen tube growth (Kaur et al. 2021). In our study, callose deposits were particularly evident on the stigmatic surface following self-crossing (Fig. 7a). For this reason, we considered it useful to investigate whether the callose accumulation observed in self-pollinated stigmas was also associated with transcriptional changes in genes encoding callose synthase. Three genes, namely L2E82_40935, L2E82_42373, and L2E82_29924, which are putative orthologues of *callose synthase 1* (*GSL6*), *7* (*GSL7*) and *3* (*GSL12*), were all significantly upregulated in the Self-P vs. Pre-P comparison. Additionally, the putative orthologous of *GSL6* was also upregulated in the Self-P vs. Cross-P comparison (Fig. 9c). Based on the TPM values, L2E82_29924 (*GSL12*) was found to be, on average, more expressed across all three tissues (i.e., 18.11, 14.47, and 3.65 for Self-P, Cross-P, and Pre-P, respectively) compared to L2E82_40935 (*GL6*) and L2E82_42373 (*GL7*), where the mean values were 2.13 (Self-P), 0.10 (Cross-P), and 0.08 (Pre-P) for the first, and 0.90 (Self-P), 0.09 (Cross-P), and 0.03 (Pre-P) for the second (Table S2). The TPM values reveal an increased expression in Self-P for all three genes.

In *Arabidopsis*, at least 12 callose synthase genes (CALS or glucan synthase-like, (GSL)) have been identified, all of which are expressed during pollen development (Ellinger and Voigt 2014). Further studies are needed to elucidate whether the increased expression of these three genes following self-pollination is indeed linked to increased callose deposition at the stigmatic level.

Among the differentially expressed transcription factors, the putative orthologous of *SEEDSTICK* (*STK,* AT4G09960), namely, L2E82_17794, is worth mentioning. The DESeq2-normalized data (Table S1), revealed that this gene has low or no expression in the leaf, pollen, or anther, whereas a transcript accumulation was observed at the stigma level prior to pollination. At this point, the amount of *STK* mRNA decreases to zero just 1 h after self-pollination, whereas it remains at high levels 1 h after cross-pollination with compatible pollen. *STK* appeared to be differentially expressed between Cross-P and Self-P (Fig. 9c). Considering the central role played by *STK* in fertilization and seed development processes (Mizzotti et al. 2012), it can be hypothesized that, following the interaction between the stigma and incompatible pollen (self), almost immediate shutdown of the gene transcription occurs.

Double fertilization, embryogenesis and embryo sac degeneration

Successful fertilization requires the guidance of the pollen tubes by the pistil, facilitating the delivery of the two generative cells (i.e., the sperm cells) from the pollen grain to the embryo sac (Raghavan 2003; Higashiyama and Takeuchi 2015; Dresselhaus et al. 2016; Adhikari et al. 2020; Shin et al. 2021). Upon reaching the micropyle of the ovule, the pollen tube passes through one of the synergids of the embryo sac and releases the two sperm cells, which then fuse with the female gametophyte (Lora et al. 2010; Palanivelu and Tsukamoto 2012; Pereira et al. 2021). The process of double fertilization represents the initial stage of seed development, a distinctive biological phenomenon wherein the destiny of two sperm nuclei is synchronized to facilitate the fertilization of two distinct cell types. The fertilization of the egg cell results in the formation of the zygote, whereas the fertilization of the homodiploid central cell fuses with the second sperm nucleus, leading to the development of the triploid endosperm. Our observations indicate that within a time frame of 5–24 h, the pollen tubes reach the ovule, thus initiating the process of double fertilization. Fertilization is micropylar, with the pollen tube entering and fusing with one of the two synergids (Fig. 10a).

This finding is consistent with ultrastructural observations in angiosperms showing that the synergid cell receiving the pollen tube undergoes programmed cell death (PCD), leading to its degeneration. This degeneration creates a passageway that facilitates sperm entry into the egg and central cells, enabling fertilization (Li et al. 2009). Calcium ion flux has been implicated in mediating this process of pollen tube reception and burst by synergids (Mascarenhas and Machlis 1962; Heslop-Harrison 1987; Higashiyama et al. 2001; Higashiyama 2002; Mendes et al. 2016).

After monitoring the pollen tube journey over a time course ranging from 20 min to 4 h, we tracked as after the pollen tubes approach the ovule, in a timeframe spanning from 5 to 96 h (five timepoints, 5 h, 24 h, 48 h, 72 h, and 96 h; Fig. 10b-f). At the same timepoints, we also examined the fate of the ovules belonging to self-pollinated plants (Fig. 10g-k). This study documents for the first time embryogenesis in chicory, starting from the zygotic stage to a fully developed embryo and endosperm, including the

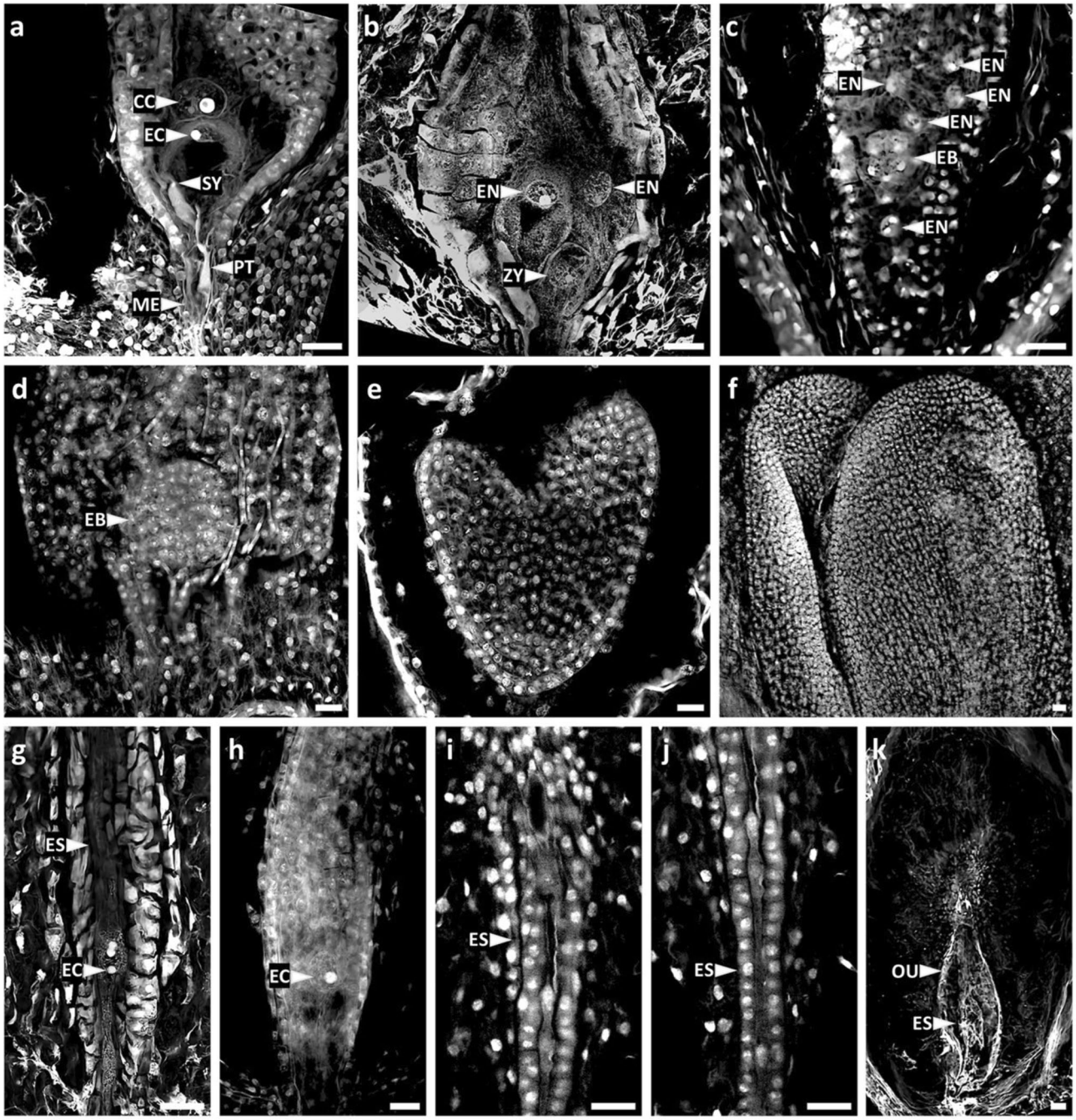

Fig. 10 Embryogenic patterns in *C. intybus*. **a** Pollen tube (*PT)* entering the micropylar end (*ME*) and fusing with one of the synergids (*SY*), image obtained from the maximum intensity Z projection. **b-f** Stages of embryogenesis in *C. intybus* after a compatible cross at five time points: **b** 5 h pp, early stages immediately after the double fertilization; zygote (*ZY*) is evident, and endosperm (*EN*) is forming; image obtained from maximum intensity Z projection; **c** 24 h pp, embryo development at 8–16 cell division stage; **d** 48 h pp, a globular embryo stage (*EB*); **e** 72 h pp, a heart-shaped embryo; and **f** 96 h pp, cotyledons at early stages of formation. **g-k** Embryo sac maturation after self-pollination at different time points. **g** After 5 h, linearly shaped embryo sac (*ES*) with well-visible egg cell (*EC*) and central cell (*CC*), was observed, and **h** after 24 h, the embryo sac with the only egg cell was still visible; the other nuclei underwent degeneration. (**i**) After 48 h, the embryo sac in which all the nuclei degenerated, **j** after 72 h, the embryo sac shrank, and **k** after 96 h the embryo sac degenerated inside the ovule (*OU)*. Scale bars: 20 µm

globular stage, heart-shaped stage, and cotyledon elongation (Fig. 10b-f). In chicory, the endosperm appears to be of the nuclear type, with endosperm nuclei undergoing rapid divisions from 5 to 24 h pp without undergoing cellularization in this timeframe (Fig. 10b, c and Supplementary Fig. 1). Like other Asteraceae (*e.g.,* in *Achillea tenuifolia*, *Hieracium*, *Pterocypsela formosana*, *Erigeron annuus*, *Chrysanthemum carinatum*, *Crepis bithynica*, *Helichrysum rupestre*, *Leontodon autumnalis*, and *Centaurea kilaea*), chicory endosperm transitions from an initial free nuclear stage to a cellular stage, after the globular stage of embryogenesis (Kapoor and Tandon 1964; Villari 1987; Yurukova-Grancharova 2004; Yurukova-Grancharova and Dimitrova 2006; Yurukova-Grancharova et al. 2006, 2012; Hua et al. 2015; Chehregani and Salehi 2016; Kartal 2025). On the other hand, a cellular type of endosperm has been documented in *Artemisia annua*, *Ambrosia artemisiifolia and Ambrosia trifida* (Chen et al. 2014; Shirkhani et al. 2024). In addition, another study in *Ambrosia artemisiifolia* reported initial free-nuclei endosperm formation, and that cellularization occurred after globular embryo formation (Yurukova-Grancharova et al. 2015). Both types of endosperm have also been documented in the *Taraxacum* genus (e.g., the nuclear type for *T. officinale* and the cellular type for T. *udum*) (van Baarlen et al. 2002; Musiał and Kościńska-Pająk 2013; Musiał et al. 2013). The variability observed at the genus (in the case of *Taraxacum*) and species levels (in the case of *Ambrosia*), appears to be a distinctive feature of the Asteraceae family. However, it cannot be ruled out that some observations may not be accurate because of difficulties in detecting and interpreting the nuclear–cellular transition of endosperm formation. Further detailed and targeted studies are needed to confirm the type of endosperm characterizing this intricate family.

Overall, our observations revealed heterogeneous stages occurring between 5 and 24 h, ranging from the entry of pollen tubes into the embryo sac to the early globular embryo stage. In some cases, delayed fertilization was noted, with pollen tubes entering the embryo sac after 24 h, whereas in other samples, endosperm cells were already observed as early as 5 h from the pollination. At the early globular stage of the embryo, several endosperm nuclei were observed, indicating a rapid division rate (Fig. 10c), whereas the globular mature embryo (Fig. 10d), was well-defined. By 72 h, various heart-shaped stages were observed, with slight differences in orientation and maturation (Fig. 10e). After 96 h, cotyledons became clearly visible (Fig. 10f).

In contrast, during self-pollination, pollen tubes rarely manage to reach the ovule, resulting in a lack of fertilization (Fig. 10g-k). In self-pollinated flowers, when no pollen tubes reach the micropylar end, the embryo sac structure begins to thin as early as 5 h after pollination. Notably, the central cell, formed by the fusion of the two polar nuclei, and the egg cell were visible and had not yet degenerated (Fig. 10g). The egg cell remained intact even after 24 h (Fig. 10h). It is hypothesized that the degeneration of antipodal and synergid cells occurs first. By 96 h, the embryo sac had degenerated completely, and its structure was no longer visible (Fig. 10k).

Conclusions

In conclusion, our findings provide new cytological insights in a research area with limited data. The application of advanced techniques, such as confocal microscopy, allowed us to elucidate for the first time the phases of megasporogenesis and megagametogenesis in *C. intybus*. Additionally, by shedding light on pollen−pistil interactions, we have added another small piece to the complex puzzle of SSI in chicory and we have established a foundation for further molecular analyses and comparative studies across the Asteraceae family. Finally, by comparing SI-mediated processes with normal embryogenesis, we have revealed key aspects of cytological dynamics that occur both in the presence and absence of fertilization. These results serve as a basis for future genetic and molecular studies, with the potential to enhance our understanding of reproductive biology in the Asteraceae family.

Supplementary Information The online version contains supplementary material available at https://doi.org/10.1007/s00299-025-03546-2.

Author contributions SD performed the experiments. SD and FP drafted the manuscript. FP and MAM coordinated the experimental data. FP, DR, and GG performed the bioinformatics analysis. AC performed the confocal microscopy analysis and image curation. FP, SF, AV, MAM and GB reviewed and edited the manuscript. All the authors contributed to the enhancement of the manuscript.

Funding This study was partially funded by the European Union—Next Generation EU, Mission 4 Component 2 Investment 1.1 CUP C53D23007660001 (Prot. P2022SK49B, call "PRIN PNRR 2022"). This study was also carried out within the Agritech National Research Center and received funding from the European Union Next-Generation EU, Mission 4 Component 2, Investment 1.4—D.D. 1032 17 June 2022, CN00000022, Task 1.3.5.

Data availability All the data analyzed during this study are included in this article and its supplementary information files. The RNA-seq datasets generated during the current study are available in the NCBI Sequence Read Archive (SRA) repository, Bioproject: PRJNA1223139, SRA: SRR32372170-SRR32372192.

Declarations

Conflict of interest No conflicts of interest are declared.

Open Access This article is licensed under a Creative Commons Attribution-NonCommercial-NoDerivatives 4.0 International License, which permits any non-commercial use, sharing, distribution and reproduction in any medium or format, as long as you give appropriate credit to the original author(s) and the source, provide a link to the Creative Commons licence, and indicate if you modified the licensed material. You do not have permission under this licence to share adapted material

derived from this article or parts of it. The images or other third party material in this article are included in the article's Creative Commons licence, unless indicated otherwise in a credit line to the material. If material is not included in the article's Creative Commons licence and your intended use is not permitted by statutory regulation or exceeds the permitted use, you will need to obtain permission directly from the copyright holder. To view a copy of this licence, visit http://creativecommons.org/licenses/by-nc-nd/4.0/.

References

Adhikari PB, Liu X, Wu X et al (2020) Fertilization in flowering plants: an odyssey of sperm cell delivery. Plant Mol Biol 103:9–32. https://doi.org/10.1007/s11103-020-00987-z

Allen AM, Lexer C, Hiscock SJ (2010) Comparative analysis of pistil transcriptomes reveals conserved and novel genes expressed in dry, wet, and semidry stigmas. Plant Physiol 154:1347–1360

Allen AM, Thorogood CJ, Hegarty MJ et al (2011) Pollen–pistil interactions and self-incompatibility in the Asteraceae: new insights from studies of *Senecio squalidus* (Oxford ragwort). Ann Bot 108:687–698

Ao C (2007) Comparative anatomy of bisexual and female florets, embryology in Calendula officinalis (Asteraceae), a naturalized horticultural plant. Sci Hortic 114:214–219

Bala M, Rehana S, Singh MP (2023) Self-incompatibility: a targeted, unexplored pre-fertilization barrier in flower crops of Asteraceae. J Plant Res 136:587–612. https://doi.org/10.1007/s10265-023-01480-6

Barcaccia G, Ghedina A, Lucchin M (2016) Current advances in genomics and breeding of leaf chicory (*Cichorium intybus* L.). Agriculture 6:50. https://doi.org/10.3390/agriculture6040050

Barrell PJ, Grossniklaus U (2005) Confocal microscopy of whole ovules for analysis of reproductive development: the *elongate1* mutant affects meiosis II. Plant J 43:309–320

Barrett SCH (2013) IV.8. Evolution of mating systems: outcrossing versus selfing. In: Losos JB, Baum DA, Futuyma DJ, et al. (eds). Princeton University Press, 356–362

Baterman RM, Di Michele WA (1994) Heterospory: the most key innovation in the evolutionary history of the plant kingdom. Biol Rev 69:345–417. https://doi.org/10.1111/j.1469-185X.1994.tb01276.x

Bawa KS, Beach JH (1981) Evolution of sexual systems in flowering plants. Ann Mo Bot Gard. https://doi.org/10.2307/2398798

Benjamini Y, Hochberg Y (1995) Controlling the false discovery rate: a practical and powerful approach to multiple testing. J R Stat Soc Series B Stat Methodol 57:289–300

Bhatla SC, Lal MA (2023) Pollination, fertilization, and seed development. Plant physiology, development and metabolism. Springer, pp 583–605

Boavida LC, Borges F, Becker JD, Feijó JA (2011) Whole genome analysis of gene expression reveals coordinated activation of signaling and metabolic pathways during pollen-pistil interactions in Arabidopsis. Plant Physiol 155:2066–2080

Botía JA, Vandrovcova J, Forabosco P et al (2017) An additional k-means clustering step improves the biological features of WGCNA gene co-expression networks. BMC Syst Biol 11:1–16

Bove J, Vaillancourt B, Kroeger J et al (2008) Magnitude and direction of vesicle dynamics in growing pollen tubes using spatiotemporal image correlation spectroscopy and fluorescence recovery after photobleaching. Plant Physiol 147:1646–1658. https://doi.org/10.1104/pp.108.120212

Burson BL (1987) Pollen germination, pollen tube growth and fertilization following self and interspecific pollination of *Paspalum* species. Euphytica 36:641–650

Castaño CI, Demeulemeester MAC, De Proft MP (1997) Incompatibility reactions and genotypic identity status of five commercial chicory (*Cichorium intybus* L.) hybrids. Sci Hortic 72:1–9. https://doi.org/10.1016/S0304-4238(97)00111-8

Chebli Y, Geitmann A (2007) Mechanical principles governing pollen tube growth. Funct Plant Sci Biotechnol 1:232–245

Chehregani A, Mohsenzadeh F, Ghanad M (2011) Male and female gametophyte development in *Cichorium intybus*.

Chehregani A, Salehi H (2016) Male and female gametophyte development in *Achillea tenuifolia* (Asteraceae). Prog Biol Sci 6:85–94

Chen B-X, Shi C-Y, Huang J-M et al (2014) Megasporogenesis, female gametophyte development and embryonic development of *Ambrosia* L. in China. Plant Syst Evol 300:197–208

Cheng C, Krishnakumar V, Chan AP et al (2017) Araport11: a complete reannotation of the *Arabidopsis thaliana* reference genome. Plant J 89:789–804

Christensen CA, King EJ, Jordan JR, Drews GN (1997) Megagametogenesis in Arabidopsis wild type and the Gf mutant. Sex Plant Reprod 10:49–64

Clifford SC, Owens SJ (1990) The stigma, style, and ovarian transmitting tract in the Oncidiinae (Orchidaceae): morphology, developmental anatomy, and histochemistry. Bot Gaz 151:440–451

Danecek P, Bonfield JK, Liddle J et al (2021) Twelve years of SAMtools and BCFtools. Gigascience 10:giab008

Darqui FS, Radonic LM, Beracochea VC et al (2021) Peculiarities of the transformation of Asteraceae family species: the cases of sunflower and lettuce. Front Plant Sci. https://doi.org/10.3389/fpls.2021.767459

De Jesús Pérez Y, Angulo MB, Honfi A, Dematteis M (2021) Embryology and fertility of the natural tetraploid Lessingianthus plantaginoides (Asteraceae, Vernonieae): taxonomic implications. Rodriguésia. https://doi.org/10.1590/2175-7860202172080

Deng Y, Chen S, Teng N et al (2010) Flower morphologic anatomy and embryological characteristics in *Chrysanthemum multicaule* (Asteraceae). Sci Hortic 124:500–505. https://doi.org/10.1016/j.scienta.2010.02.009

Dickinson H (1995) Dry stigmas, water and self-incompatibility in *Brassica*. Sex Plant Reprod 8:1–10

Dresselhaus T, Sprunck S, Wessel GM (2016) Fertilization mechanisms in flowering plants. Curr Biol 26:R125–R139

Drews GN, Koltunow AMG (2011) The female gametophyte. Arabidopsis Book 9:e0155. https://doi.org/10.1199/tab.0155

Drews GN, Yadegari R (2002) Development and function of the angiosperm female gametophyte. Annu Rev Genet 36:99–124

Eenink AH (1981) Compatibility and incompatibility in witloof-chicory (*Cichorium intybus* L.). 1. The influence of temperature and plant age on pollen germination and seed production. Euphytica 30:71–76

Elias RA, Lando AP, Viana WG et al (2019) Structural aspects of cypsela and seed development of *Trichocline catharinensis* (Cabrera): a Brazilian endemic species. Protoplasma 256:1495–1506. https://doi.org/10.1007/s00709-019-01361-7

Elleman CJ, Franklin-Tong V, Dickinson HG (1992) Pollination in species with dry stigmas: the nature of the early stigmatic response and the pathway taken by pollen tubes. New Phytol 121:413–424

Ellinger D, Voigt CA (2014) Callose biosynthesis in Arabidopsis with a focus on pathogen response: what we have learned within the last decade. Ann Bot 114:1349–1358

Eschrich W, Currier HB (1964) Identification of cauose by its diachrome and fluorochrome reactions. Stain Technol 39:303–307. https://doi.org/10.3109/10520296409061248

Ewels P, Magnusson M, Lundin S, Käller M (2016) MultiQC: summarize analysis results for multiple tools and samples in a single report. Bioinformatics 32:3047–3048

Faehnrich B, Kraxner C, Kummer S, Franz C (2015) Pollen tube growth and self incompatibility in *Matricaria recutita*. Euphytica 206:357–363

Fan W, Wang S, Wang H et al (2022) The genomes of chicory, endive, great burdock and yacon provide insights into Asteraceae palaeo-polyploidization history and plant inulin production. Mol Ecol Resour 22:3124–3140

Forrest JRK (2014) Plant size, sexual selection, and the evolution of protandry in dioecious plants. Am Nat 184:338–351

Franca RDO, De-Paula OC, Carmo-Oliveira R, Marzinek J (2015) Embryology of *Ageratum conyzoides* L. and A. fastigiatum RM king & H. rob. (Asteraceae). Acta Bot Brasilica 29:8–15

Funk VA, Bayer RJ, Keeley S et al (2005) Everywhere but Antarctica: Using a super tree to understand the diversity and distribution of the compositae. Biol Skr 55:343–373

Galen C, Gregory T, Galloway LF (1989) Costs of self-pollination in a self-incompatible plant, *Polemonium viscosum*. Am J Bot 76:1675–1680

Gao H, Li R, Guo Y (2017) Arabidopsis aspartic proteases A36 and A39 play roles in plant reproduction. Plant Signal Behav 12:e1304343

Ge SX, Jung D, Yao R (2020) ShinyGO: a graphical gene-set enrichment tool for animals and plants. Bioinformatics 36:2628–2629

Gotelli MM, Galati BG, Medan D (2008) Embryology of *Helianthus annuus* (Asteraceae). Annales botanici fennici. BioOne, pp 81–96

Grossniklaus U, Schneitz K (1998) The molecular and genetic basis of ovule and megagametophyte development. Seminars in cell & developmental biology. Elsevier, pp 227–238

Habarugira I, Hendriks T, Quillet M-C et al (2015) Effects of nuclear genomes on anther development in cytoplasmic male sterile chicories (*Cichorium intybus* L.): morphological analysis. Sci World J 2015:529521

Hepler PK, Rounds CM, Winship LJ (2013) Control of cell wall extensibility during pollen tube growth. Mol Plant 6:998–1017

Heslop-Harrison J (1987) Pollen germination and pollen-tube growth. International review of cytology. Elsevier, pp 1–78

Heslop-Harrison Y, Shivanna KR (1977) The receptive surface of the angiosperm stigma. Ann Bot 41:1233–1258

Heydlauff J, Groß-Hardt R (2014) Love is a battlefield: programmed cell death during fertilization. J Exp Bot 65:1323–1330

Higashiyama T (2002) The synergid cell: attractor and acceptor of the pollen tube for double fertilization. J Plant Res 115:149–160

Higashiyama T, Takeuchi H (2015) The mechanism and key molecules involved in pollen tube guidance. Annu Rev Plant Biol 66:393–413. https://doi.org/10.1146/annurev-arplant-043014-115635

Higashiyama T, Yabe S, Sasaki N et al (2001) Pollen tube attraction by the synergid cell. Science 293:1480–1483

Hiscock SJ, Allen AM (2008) Diverse cell signalling pathways regulate pollen-stigma interactions: the search for consensus. New Phytol 179:286–317

Hiscock SJ, Hoedemaekers K, Friedman WE, Dickinson HG (2002) The stigma surface and pollen-stigma interactions in *Senecio squalidus* L. (Asteraceae) following cross (compatible) and self (incompatible) pollinations. Int J Plant Sci 163:1–16

Hua L, Ma X, Huang H (2015) Studies on sexual organs and embryological development morphology of *Pterocypsela formosana*. Zhongguo Zhong Yao Za Zhi 40:198–203

Janas A, Musiał K, Kościńska-Pająk M, Marciniuk P (2016) Insights into developmental processes in anthers, ovaries, and ovules of *Taraxacum belorussicum* (Asteraceae-Cichorioideae) using DIC optics. Plant Syst Evol 302:617–628. https://doi.org/10.1007/s00606-016-1288-4

Janas AB, Szeląg Z, Musiał K (2021) In search of female sterility causes in the tetraploid and pentaploid cytotype of *Pilosella brzovecensis* (Asteraceae). J Plant Res 134:803–810. https://doi.org/10.1007/s10265-021-01290-8

Johri BM, Ambegaokar KB, Srivastava PS (2013) Comparative embryology of angiosperms, vol 1/2. Springer Science & Business Media

Kägi C, Baumann N, Nielsen N et al (2010) The gametic central cell of Arabidopsis determines the lifespan of adjacent accessory cells. Proc Natl Acad Sci U S A 107:22350–22355

Kaothien-Nakayama P, Isogai A, Takayama S (2010) Self-Incompatibility Systems in Flowering Plants. In: Pua EC, Davey MR (eds) Plant developmental biology - biotechnological perspectives, vol 1. Springer Berlin Heidelberg, Berlin, Heidelberg, pp 459–485

Kapoor K, Geitmann A (2023) Pollen tube invasive growth is promoted by callose. Plant Reprod 36:157–171. https://doi.org/10.1007/s00497-023-00458-7

Kapoor BM, Tandon SL (1964) Contributions to the cytology of endosperm in some angiosperms-VIII. *Chrysanthemum carinatum* L. Genetica 35:197–204

Kartal C (2025) Reproductive biology of *Centaurea kilaea* (Asteraceae, Cardueae)–an endemic species from Türkiye. Acta Bot Croat. https://doi.org/10.37427/botcro-2025-003

Kaur K, Gupta M, Vikal Y et al (2021) Callose depositions underlie the incompatible reaction in intergeneric crosses of rice. Plant Genet Resour 19:447–452

Langfelder P, Horvath S (2008) WGCNA: an R package for weighted correlation network analysis. BMC Bioinform 9:1–13

Langmead B, Salzberg SL (2012) Fast gapped-read alignment with Bowtie 2. Nat Methods 9:357–359

Lawrence M, Huber W, Pagès H et al (2013) Software for computing and annotating genomic ranges. PLoS Comput Biol 9:e1003118

Leduc N, Douglas GC, Monnier M, Connolly V (1990) Pollination in vitro: effects on the growth of pollen tubes, seed set and gametophytic self-incompatibility in *Trifolium pratense* L. and *T. repens* L. Theor Appl Genet 80:657–664

Li DX, Lin MZ, Wang YY, Tian HQ (2009) Synergid: a key link in fertilization of angiosperms. Biol Plant 53:401–407

Li H-J, Zhu S-S, Zhang M-X et al (2015) *Arabidopsis* CBP1 is a novel regulator of transcription initiation in central cell-mediated pollen tube guidance. Plant Cell 27:2880–2893

Liu J, Zhong S, Guo X et al (2013) Membrane-bound RLCKs LIP1 and LIP2 are essential male factors controlling male-female attraction in *Arabidopsis*. Curr Biol 23:993–998

Lloyd DG (1968) Pollen tube growth and seed set in self-incompatible and self-compatible Leavenworthia (Cruciferae) populations. New Phytol 67:179–195

Lloyd DG, Webb CJ (1977) Secondary sex characters in plants. Bot Rev 43:177–216

Lora J, Hormaza JI, Herrero M (2010) The progamic phase of an early-divergent angiosperm, Annona cherimola (Annonaceae). Ann Bot 105:221–231. https://doi.org/10.1093/aob/mcp276

Love MI, Huber W, Anders S (2014) Moderated estimation of fold change and dispersion for RNA-seq data with DESeq2. Genome Biol 15:1–21

Love J, Graham SW, Irwin JA et al (2016) Self-pollination, style length development and seed set in self-compatible Asteraceae: evidence from *Senecio vulgaris* L. Plant Ecol Divers 9:371–379

Lucchin M, Varotto S, Barcaccia G, Parrini P (2008) Chicory and endive. In: Prohens J, Nuez F (eds) Vegetables I: Asteraceae, Brassicaceae, Chenopodicaceae, and Cucurbitaceae. Springer New York, New York, NY, pp 3–48

M Kiers A (2000) Endive, chicory, and their wild relatives. a systematic and phylogenetic study of Cichorium (Asteraceae). Gorteria Dutch Bot Arch-Suppl 5:1–77

Martin M (2011) Cutadapt removes adapter sequences from high-throughput sequencing reads. Embnet J 17:10–12

Martinoli G, Di Moisè BA (1963) Ricerche Embriologiche su *Senecio vulgaris* L. var. Thyrrenus Fiori. G Bot Ital 70:482–492. https://doi.org/10.1080/11263506309434953

Maruyama D, Higashiyama T (2016) The end of temptation: the elimination of persistent synergid cell identity. Curr Opin Plant Biol 34:122–126. https://doi.org/10.1016/j.pbi.2016.10.011

Mascarenhas JP, Machlis L (1962) Chemotropic response of Antirrhinum majus pollen to calcium. Nature 196:292–293

Mason KN, Ekanayake G, Heese A (2020) Chapter 10 - staining and automated image quantification of callose in *Arabidopsis* cotyledons and leaves. In: Anderson CT, Haswell ES, Dixit R (eds) Methods in cell biology. Academic Press, pp 181–199

Mathieu A-S, Périlleux C, Jacquemin G et al (2020) Impact of vernalization and heat on flowering induction, development and fertility in root chicory (*Cichorium intybus* L. var. sativum). J Plant Physiol 254:153272. https://doi.org/10.1016/j.jplph.2020.153272

Mendes MA, Guerra RF, Castelnovo B et al (2016) Live and let die: a REM complex promotes fertilization through synergid cell death in Arabidopsis. Development 143:2780–2790

Mergner J, Frejno M, List M et al (2020) Mass-spectrometry-based draft of the Arabidopsis proteome. Nature 579:409–414

Mizzotti C, Mendes MA, Caporali E et al (2012) The MADS box genes SEEDSTICK and ARABIDOPSIS Bsister play a maternal role in fertilization and seed development. Plant J 70:409–420

Mogensen HL (1984) Quantitative observations on the pattern of synergid degeneration in barley. Am J Bot 71:1448–1451. https://doi.org/10.1002/j.1537-2197.1984.tb12002.x

Mondragón-Palomino M, John-Arputharaj A, Pallmann M, Dresselhaus T (2017) Similarities between reproductive and immune pistil transcriptomes of Arabidopsis species. Plant Physiol 174:1559–1575

Musiał K, Kościńska-Pająk M (2013) Egg apparatus in sexual and apomictic species of Taraxacum: structural and immunocytochemical aspects of synergid cells. Acta Biol Crac Bot. https://doi.org/10.2478/abcsb-2013-00011

Musiał K, Górka P, Kościńska-Pająk M, Marciniuk P (2013) Embryological studies in *Taraxacum udum* Jordan (sect. Palustria). Botany 91:614–620. https://doi.org/10.1139/cjb-2013-0022

Nasrallah JB (2023) Stop and go signals at the stigma–pollen interface of the Brassicaceae. Plant Physiol 193:927–948

Noyes RD, Allison JR (2005) Cytology, ovule development, and pollen quality in sexual *Erigeron strigosus* (Asteraceae). Int J Plant Sci 166:49–59. https://doi.org/10.1086/425670

Pacini E, Keijzer CJ (1989) Ontogeny of intruding non-periplasmodial tapetum in the wild chicory,*Cichorium intybus* (Compositae). Plant Syst Evol 167:149–164. https://doi.org/10.1007/BF00936403

Pacini E, Nepi M, Vesprini JL (2003) Nectar biodiversity: a short review. Plant Syst Evol 238:7–21

Pagnussat GC, Alandete-Saez M, Bowman JL, Sundaresan V (2009) Auxin-dependent patterning and gamete specification in the *Arabidopsis* female gametophyte. Science 324:1684–1689

Palanivelu R, Tsukamoto T (2012) Pathfinding in angiosperm reproduction: pollen tube guidance by pistils ensures successful double fertilization. Wires Dev Biol 1:96–113

Palanivelu R, Brass L, Edlund AF, Preuss D (2003) Pollen tube growth and guidance is regulated by POP2, an Arabidopsis gene that controls GABA levels. Cell 114:47–59

Pang C-C, Saunders RMK (2014) The evolution of alternative mechanisms that promote outcrossing in Annonaceae, a self-compatible family of early-divergent angiosperms. Bot J Linn Soc 174:93–109. https://doi.org/10.1111/boj.12118

Peñas J, Lorite J, Alba-Sánchez F, Taisma MA (2011) Self-incompatibility, floral parameters, and pollen characterization in the narrow endemic and threatened species *Artemisia granatensis* (Asteraceae). An Jard Bot Madrid. https://doi.org/10.3989/ajbm.2276

Pereira AM, Moreira D, Coimbra S, Masiero S (2021) Paving the way for fertilization: the role of the transmitting tract. Int J Mol Sci 22:2603

Petersen KB, Burd M (2017) Why did heterospory evolve? Biol Rev 92:1739–1754. https://doi.org/10.1111/brv.12304

Qin Y, Leydon AR, Manziello A et al (2009) Penetration of the stigma and style elicits a novel transcriptome in pollen tubes, pointing to genes critical for growth in a pistil. PLoS Genet 5:e1000621

Quinlan AR, Hall IM (2010) BEDtools: a flexible suite of utilities for comparing genomic features. Bioinformatics 26:841–842

Raghavan V (2003) Some reflections on double fertilization, from its discovery to the present. New Phytol 159:565–583. https://doi.org/10.1046/j.1469-8137.2003.00846.x

Rejón JD, Delalande F, Schaeffer-Reiss C et al (2014) The plant stigma exudate: a biochemically active extracellular environment for pollen germination? Plant Signal Behav 9:5695–5705

Rong D, Luo N, Mollet JC et al (2016) Salicylic acid regulates pollen tip growth through an NPR3/NPR4-independent pathway. Mol Plant 9:1478–1491

Samaha RR, Boyle TH, Mulcahy DL (1989) Self-incompatibility of Zinnia angustifolia HBK (compositae) i. application of visible light and fluorescence microscopy for assessment of self-incompatibility. Sex Plant Reprod 2:18–26

Sang YL, Xu M, Ma FF et al (2012) Comparative proteomic analysis reveals similar and distinct features of proteins in dry and wet stigmas. Proteomics 12:1983–1998

Schneider CA, Rasband WS, Eliceiri KW (2012) NIH image to ImageJ: 25 years of image analysis. Nat Methods 9:671–675. https://doi.org/10.1038/nmeth.2089

Sharma B, Bhatla SC (2013) Structural analysis of stigma development in relation with pollen–stigma interaction in sunflower. Flora - Morphol, Distrib, Funct Ecol Plants 208:420–429. https://doi.org/10.1016/j.flora.2013.07.003

Shin JM, Yuan L, Ohme-Takagi M, Kawashima T (2021) Cellular dynamics of double fertilization and early embryogenesis in flowering plants. J Exp Zool B Mol Dev Evol 336:642–651. https://doi.org/10.1002/jez.b.22981

Shirkhani Z, Chehregani Rad A, Mohsenzadeh F (2024) Developmental and systematic value of flower reproductive organs in *Artemisia annua*. Rostaniha 25:49–68

Song X, Yuan L, Sundaresan V (2014) Antipodal cells persist through fertilization in the female gametophyte of Arabidopsis. Plant Reprod 27:197–203

Sprunck S, Groß-Hardt R (2011) Nuclear behavior, cell polarity, and cell specification in the female gametophyte. Sex Plant Reprod 24:123–136

Sulborska A (2011) Micromorphology of flowers, anatomy and ultrastructure of *Chamomilla recutita* (L.) Rausch. (Asteraceae) nectary. Acta Agrobot 64:23–34

Sulborska A, Weryszko-Chmielewska E (2007) Anatomy and ultrastructure of floral nectary of *Inula helenium* L.[Asteraceae]. Acta Soc Bot Pol 76:201–207

Sun Y, Wang X, Pan L et al (2021) Plant egg cell fate determination depends on its exact position in female gametophyte. Proc Natl Acad Sci U S A 118:e2017488118

Teixeira SDP, Capucho LC, Machado SR (2011) Two novel reports of semidry stigmatic surface in Asteraceae. Flora - Morphol, Distrib, Funct Ecol Plants 206:328–333. https://doi.org/10.1016/j.flora.2010.08.001

van Baarlen P, de Jong HJ, van Dijk PJ (2002) Comparative cytoembryological investigations of sexual and apomictic dandelions (Taraxacum) and their apomictic hybrids. Sex Plant Reprod 15:31–38

Van Hautegem T, Waters AJ, Goodrich J, Nowack MK (2015) Only in dying, life: programmed cell death during plant development. Trends Plant Sci 20:102–113

Varotto S, Pizzoli L, Lucchin M, Parrini P (1995) The incompatibility system in Italian red chicory (*Cichorium intybus* L.). Plant Breed 114:535–538

Varotto S, Parrini P, Mariani P (1996) Pollen ontogeny in *Cichorium intybus* L. Grana 35:154–161. https://doi.org/10.1080/00173139609429076

Villari R (1987) Embryology of Helichrysum rupestre (Rafin.) DC. var. messerii Pignatti (Inuleae, Asteraceae). G Bot Ital 121:27–40

Waegneer E, Rombauts S, Baert J et al (2023) Industrial chicory genome gives insights into the molecular timetable of anther development and male sterility. Front Plant Sci. https://doi.org/10.3389/fpls.2023.1181529

Weterings K, Pezzotti M, Cornelissen M, Mariani C (2002) Dynamic 1-aminocyclopropane-1-carboxylate-synthase and -oxidase transcript accumulation patterns during pollen tube growth in tobacco styles. Plant Physiol 130:1190–1200

Wist TJ, Davis AR (2008) Floral structure and dynamics of nectar production in Echinacea pallida var. angustifolia (asteraceae). Int J Plant Sci 169:708–722. https://doi.org/10.1086/533602

Wojtaszek JW, Maier C (2014) A microscopic review of the sunflower and honeybee mutualistic relationship.

Wu S-W, Kumar R, Iswanto ABB, Kim J-Y (2018) Callose balancing at plasmodesmata. J Exp Bot 69:5325–5339

Yadegari R, Drews GN (2004) Female gametophyte development. Plant Cell 16:S133–S141

Yang W-C, Sundaresan V (2000) Genetics of gametophyte biogenesis in Arabidopsis. Curr Opin Plant Biol 3:53–57

Yurukova-Grancharova PD (2004) On the embryology of *Leontodon autumnalis* (Asteraceae). Phytol Balc (Sofia) 10:85–91

Yurukova-Grancharova P, Dimitrova D (2006) Cytoembryological study of *Crepis bithynica* (Asteraceae) from Bulgaria. Flora Mediterr 16:33–43

Yurukova-Grancharova P, Robeva-Davidova P, Vladimirov V (2006) On the embryology and mode of reproduction of selected diploid species of *Hieracium* sl (Asteraceae) from Bulgaria. Flora-Morphol, Distrib, Funct Ecol Plants 201:668–675

Yurukova-Grancharova P, Yankova-Tsvetkova E, Baldjiev G, Vladimirov V (2012) On the reproductive biology of the invasive alien species *Erigeron annuus* (Asteraceae) in the Bulgarian flora. Comptes Rendus De L'Acad Bulg Sci 65:933–938

Yurukova-Grancharova P, Yankova-Tsvetkova E, Baldjiev G, Vladimirov V (2015) Reproductive characteristics of *Ambrosia artemisiifolia* and Iva xanthiifolia–two Invasive alien species in Bulgaria. Comptes Rendus De l'Académie Bul Des Sci 68:853–862

Zhang T, Gao C, Yue Y et al (2017) Time-course transcriptome analysis of compatible and incompatible pollen-stigma interactions in *Brassica napus* L. Front Plant Sci 8:682

Zheng Y-Y, Lin X-J, Liang H-M et al (2018) The long journey of pollen tube in the pistil. Int J Mol Sci 19:3529

Publisher's Note Springer Nature remains neutral with regard to jurisdictional claims in published maps and institutional affiliations.